Available online at www.sciencedirect.com
ScienceDirect
Precambrian Research 149 (2006) 126–148
Precambrian Research
www.elsevier.com/locate/precamres

Ediacaran fossil preservation: Taphonomy and diagenesis of a discoid biota from the Amadeus Basin, central Australia

N.B. Mapstone [a,*], D. McIlroy [b]

[a] School of Earth Sciences, Birkbeck University of London, Malet Street, London WC1E 7HX, UK
[b] Department of Earth Sciences, Memorial University of Newfoundland, St John's, Newfoundland A1B 3X5, Canada

Received 18 November 2005; received in revised form 8 May 2006; accepted 15 May 2006

Abstract

Aspects of the preservation of the enigmatic soft-bodied Ediacara biota in relatively coarse-grained siliciclastic sediments remain unresolved. The taphonomic model proposed by Gehling in 1999 is here validated through examination of previously unpublished discoid fossils from the shallow marine-deltaic Arumbera Sandstone in the Amadeus Basin. Within the Flinders-style preservation, the model predicts stalked-frondose organisms attached by a discoid-holdfast to a microbial mat encrusted sea-bed, with sedimentation as periodic storm-event beds during a terminal Neoproterozoic taphonomic window. A pyrite sole-veneer provided critical fossil rigidity during burial. The sequence of sedimentation events presented here advances a slightly modified Gehling model. No direct evidence of pyrite is detected; instead, a thin haematite/clay coating covers fossil hyporelief surfaces. Nevertheless, an original pyrite sole-veneer is indirectly validated by tracing its diagenetic history through to today's haematite. Detailed petrography demonstrates reducing conditions during eodiagenesis that remained anoxic mildly alkaline through mesodiagenesis, thus the pyrite sole-veneer survived deepest burial. Meteoric water penetrated the deep regolith during prolonged telodiagenesis creating oxic mildly acidic pore-water, so pyrite oxidised and hydrolised to haematite. The applicability of Gehling's model is higher where marine shelf sediments subsided continuously. In shallower or eroded areas that experienced intermittent meteoric eodiagenesis, diagenetic history was different and Ediacaran fossil preservation unlikely. Diagenetic history, therefore, has crucial implications for Ediacaran fossil preservation.

Keywords: Ediacaran; Amadeus Basin; Discoid fossils; Taphonomy; Sole-veneer; Diagenesis

1. Introduction

The late-Neoproterozoic and Cambrian was a period of fundamental change on Earth following the breakup of Rodinia and the early stages in the formation of Gondwana (Dalziel, 1997; Meert and Lieberman, 2004), global 'snowball' glaciations (Hoffman et al., 1998; Walter and Veevers, 2000; Hyde et al., 2000; Schaefer and Burgess, 2003), and major changes in ocean and atmospheric chemistry (Knoll and Walter, 1992; Brasier, 1992; Bartley et al., 1998). Increased trace fossil diversity reflects the early evolution and diversification of the Metazoa, and begins during the Ediacaran Period (Knoll et al., 2004) with the enigmatic Ediacara biota (575–542 Ma). The acme of diverse Ediacaran organisms was the final 20 Ma of that period. Ediacaran fossils are recorded from over 30 localities on five continents (Narbonne, 1998), of which the four most studied localities are the Flinders Ranges in South Australia, the Avalon Penninsula of southeastern Newfoundland, the White Sea coast in northern Russia, and southern Namibia.

* Corresponding author. Tel.: +44 1483 472194
E-mail address: mapstone@btinternet.com (N.B. Mapstone).

0301-9268/$ – see front matter © 2006 Elsevier B.V. All rights reserved.
doi:10.1016/j.precamres.2006.05.007

The Ediacara biota was dominated by discoid, stalked-frondose, flat-reclining and segmented morphological forms. Early discoveries were assigned to scyphozoan jellyfish and frond-like benthic pennatulaceans (Sprigg, 1947, 1949; Glaessner, 1959, 1979, 1984; Glaessner and Wade, 1966; Wade, 1968, 1972). Subsequent research (Gehling, 1991, 1999; Jenkins, 1992, 1995; Narbonne, 1998) mainly accepted the discoid and stalked-frondose forms as parts of pennatulacean sea-pens attached to the seabed by a bulbous holdfast. Most commonly, discoid and stalked-frondose forms are fossilised separately; rarely, excellent examples occur intact (Jenkins and Gehling, 1978; Seilacher, 1992; LaFlamme et al., 2004; Narbonne, 2004). An intergrading plexus of three end-member discoid morphs representing different preservation states of the single Ediacaran taxon *Aspidella* Billings, 1872 is proposed by Gehling et al. (2000), who suggest that the well known discoids *Ediacaria*, *Cyclomedusa* and others are junior synonyms of *Aspidella*. Other researchers suggest disparate affinities for elements of the Ediacara biota, from microbial growths to giant protists, a subject addressed in the recent comprehensive review of the Ediacara biota by Narbonne (2005). A radical interpretation proffered by Seilacher (1984, 1989, 1992) introduced the unconventional quilted pneu construction for frondose and segmented forms within an extinct kingdom Vendobionta (later phylum Vendobionta, Buss and Seilacher, 1994). Despite the general lack of enthusiasm for Seilacher's ideas, latest research resurrects this modular construction of self-similar highly fractal elements called rangeomorph frondlets (Brasier and Antcliffe, 2004; Narbonne, 2004; Xiao et al., 2005). Intergrading rangeomorph frondlets combined in various ways to build different segmented frond-, bush-, plume-, comb- or spindle-shaped morphology, some of which are fossilised with a discoid-holdfast. Nevertheless, Narbonne (2005) still allies the frond, stalk and discoid-holdfast organism *Charniodiscus* with crown-group cnidarians, but all other rangeomorph based forms he regards as a 'forgotten' architecture representing an extinct phylum-level stem-group indistinguishable from Seilacher's Vendobionta. Rare Cambrian frondose survivors are also likened to Ediacaran vendobionts (Shu et al., 2006).

At most Ediacaran localities worldwide the ongoing palaeontological enigma is why and how this soft-bodied biota was preserved in relatively coarse-grained siliciclastic sediments under high-energy conditions? Four discrete preservational styles are proposed for the Ediacara biota based on a worldwide review (Narbonne, 2005). Narbonne's 'Flinders-style preservation' applies to Ediacaran shallow marine and deltaic deposits in the White Sea and Flinders Ranges, and incorporates Gehling's (1999) pyrite sole-veneer taphonomic model. The present paper addresses this enigma, and argues the case that a slightly modified Gehling (1999) model also applies to the preservation of Ediacaran discoid fossils within the Arumbera Sandstone from the Amadeus Basin, central Australia. Furthermore, we demonstrate petrographically how diagenesis initially retained, but subsequently modified, original fossil preservation.

2. Geological setting

2.1. Amadeus Basin structural evolution

The Amadeus Basin (Fig. 1a and b) contains a Neoproterozoic-Palaeozoic shallow marine to fluvial succession of clastic, evaporate and carbonate sediments (Lindsay, 1987) and is one of several similar tenuously interconnected basins forming the Centralian Superbasin of Australia (Walter and Veevers, 2000). The Ooraminna Sub-basin occupies the north-eastern part of the Amadeus Basin (Fig. 1b and c), to the west is the saddle-shaped Missionary Plain Trough where the succession is thinner and some formations absent, and further west the Carmichael Sub-basin. The Petermann Ranges Orogeny (c.580–530 Ma) to south-west of the Amadeus Basin (Fig. 1b) was either synchronous with (Lindsay and Korsch, 1989, 1991) or slightly earlier than (Oaks et al., 1991; Shaw, 1991) the Neoproterozoic–Cambrian transition. By the Silurian, however, marine sedimentation was limited to the periphery of equatorial Australia while the centre of the craton experienced non-marine syntectonic 'molasse' deposition through to the Devonian. The basin was terminally disrupted by the Alice Springs Orogeny (Devonian to early Carboniferous) when thrusting and folding caused 50–100 km of basin shortening (Lindsay and Korsch, 1991; Lindsay, 1993), during which the current basin outline formed, including the high escarpments of the Macdonnell Ranges east and west of Alice Springs. By the Carboniferous, the Australian continent was an established subaerial landmass as part of the Gondwanan portion of Pangea. No significant sedimentation or tectonism has occurred since that time, so most of central Australia, including the Amadeus Basin, was a land area since as far back as the Silurian.

2.2. Arumbera Sandstone stratigraphy and sedimentation

The Arumbera Sandstone straddles the Neoproterozoic–Cambrian transition and was deposited as two

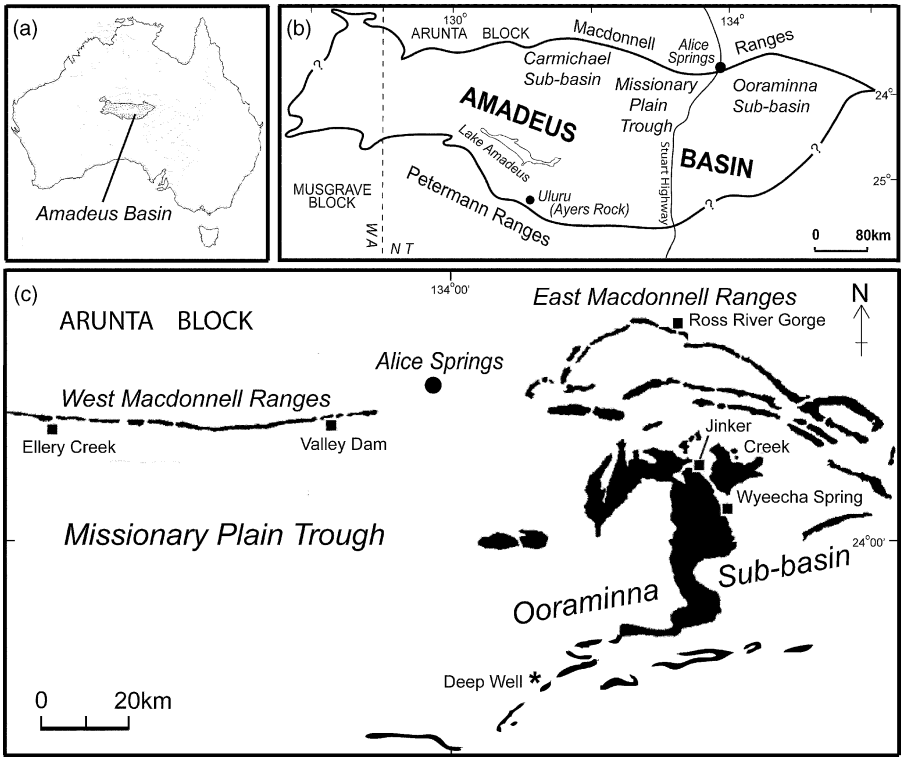

Fig. 1. Location maps. (a) The Amadeus Basin is an intracratonic basin initiated about 900 Ma; (b) and (c) Arumbera Sandstone outcrop (black ornament) and the sub-basins in the north-eastern Amadeus Basin; the Petermann Ranges were the Neoproterozoic–Cambrian provenance; sample locations indicated by black squares in (c); float sample of *Rangia* frond located near Deep Well and figured by Glaessner (1969, Fig. 9) indicated as asterisk. (a) Derived from Lindsay et al. (1987, Fig. 1); (b) derived from Lindsay (1987, Fig. 1); (c) derived from McIlroy et al. (1997, Fig. 1) and Lindsay (1993, Plate 13).

major shallow marine and deltaic sequences (Fig. 2) in the Ooraminna and Carmichael Sub-basins and in part over the Missionary Plain Trough (Lindsay, 1987; Lindsay and Korsch, 1989, 1991). Sediment provenance was the Petermann Ranges to the south-west (Fig. 1b) with sediment transported in heavily laden braided streams. Coarse arkosic conglomerate at Uluru (Ayers Rock) is the proximal equivalent of the distal Arumbera Sandstone (Lindsay and Korsch, 1991).

The Arumbera Sandstone comprises four lithological sub-divisions numbered from the base upward (Wells et al., 1967). These four units and the overlying Todd River Dolomite together make up two mappable seismic sequences. Each sequence has a lower fine-grained recessive portion (Members I and III) overlain by massive resistant sandstone (Members II and IV). We maintain the informal member notation (McIlroy et al., 1997). Sequence-1 represents a large-scale coarsening-upward cycle, with deposition as small-scale deltas prograding across the underlying carbonate platform. Sequence-2 is also a coarsening-upward cycle, but was deposited in major deltaic complexes prograding at the sub-basin scale. Seismic data demonstrate prograding clinoforms (Lindsay and Korsch, 1991; Lindsay, 1993). The recessive Members I and III consist of pro-delta silty shale overlain by thinly interbedded repetitions of shale, siltstone and fine-grained arkosic sandstone. The sandstones become coarser-grained, increase in number and thickness up-section, and were deposited in a mid-upper delta-front environment and reflect storm-flood events. Members II and IV are massive cliff forming fine-coarse grained arkosic sandstone that formed on a delta-coastal plain and delta-top with laterally restricted distributary channels. The Todd River Dolomite is an interbedded carbonate and siliciclastic tidal flat deposit (Lindsay, 1987), overlain by archaeocyathan bioherms and stratiform stromatolites (Lindsay and Gorter, 1992).

Traditionally, the Neoproterozoic–Cambrian boundary is positioned between the top of the massive Member II sandstone and the base of the recessive Member III

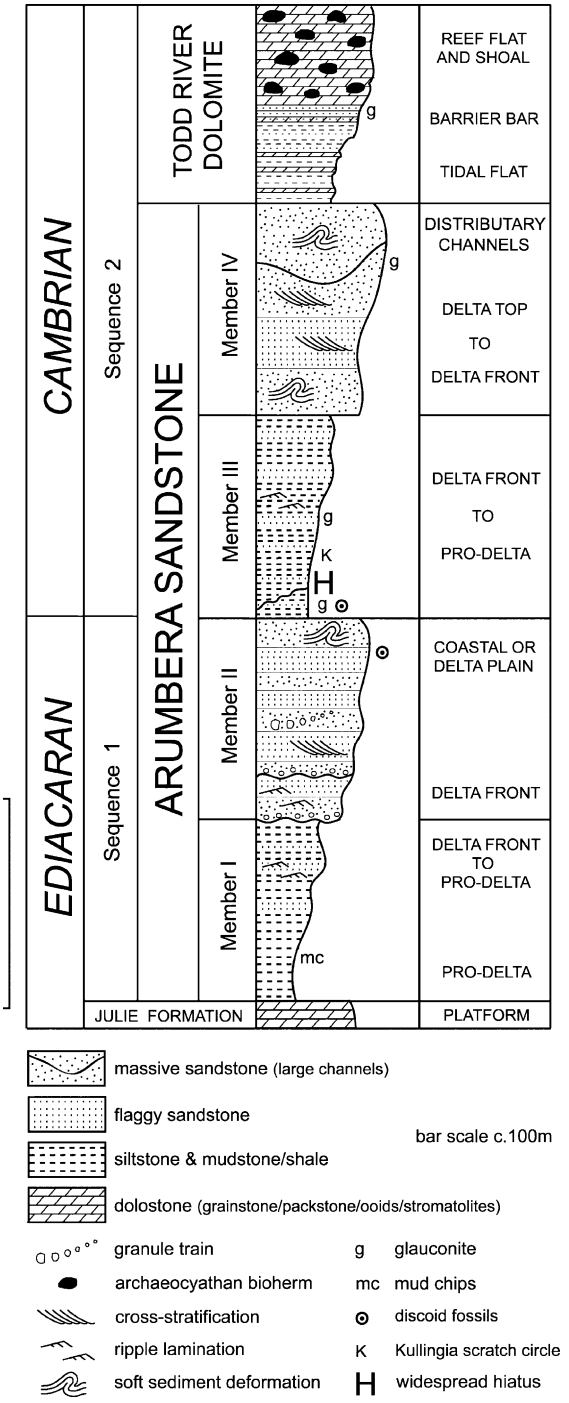

Fig. 2. Arumbera Sandstone lithostratigraphy in the Ooraminna Subbasin, illustrates the two depositional sequences, four informal lithological members, depositional environments, and location of discoid fossils and Kullingia scratch circles. Section compiled from: Members I & II after Mapstone (unpublished MRes thesis, University of London, 2004); Members III and lowermost IV after McIlroy et al. (1997, Fig. 10); remainder and general style after Lindsay (1987, Fig. 4) and Lindsay and Gorter (1992, Fig. 3.9); the widespread hiatus H after McIlroy et al. (1997, Fig. 2).

(Lindsay, 1987, 1993; Lindsay and Gorter, 1992). This traditional view is questioned by McIlroy et al. (1997) and, from inspection of numerous outcrops in the north-east of the basin, instead position the boundary at an erosional hiatus 12–25 m above the base of recessive Member III (Fig. 2, marked H). Consequently, our main fossiliferous horizon 7 m above the base of Member III at Wyeecha Spring is either earliest Cambrian (the traditional view) or very latest Neoproterozoic (the McIlroy et al., 1997 view).

2.3. Arumbera Sandstone palaeontology

The first reference to discoid fossils in central Australia is Wade (1969) who describes scyphozoan-grade medusoids *Hallidaya* and *Skinnera* some 170 km NNE of Alice Springs, effectively the south-western margin of the adjacent Georgina Basin. *Hallidaya* was also found within the Amadeus Basin, 23 km WSW of Alice Springs (Wade, 1969); this occurrence is interpreted as part of Arumbera Sandstone Member II by Shergold (1991), and inferred as latest Neoproterozoic by McIlroy et al. (1997) in their Valley Dam description.

An incomplete frond of *Rangea* cf. *longa* is recorded from talus '*near the base*' of the Arumbera Sandstone 80 km SSE of Alice Springs adjacent to the Deep Well location (Glaessner, 1969; Wade, 1970; Fig. 1c). This specimen was referred to *Rangea arborea* in Wells et al. (1970), and later to *Charniodiscus* (Waggoner's, 2003 database).

Ediacaran fossils assign a probable Neoproterozoic age to Members I and II, trace fossils indicate an early Cambrian age for Member III, whilst the Todd River Dolomite archaeocyathan faunas are late Atdabanian to early Botomian in age.

The pseudofossil Kullingia is recorded from several locations within the Arumbera Sandstone (McIlroy et al., 1997). The former discoid fossil described as *Kullingia concentrica* Glaessner by Føyn and Glaessner (1979) is re-interpreted, based on material from northern Sweden, as a wave induced scratch circle formed by the sweeping motion of the frond or stalk of an anchored pennatulid or tubular organism (Jensen et al., 2002) or perhaps a macrophytic alga. Occurrences of Kullingia scratch circles from northern Sweden, including those originally assigned a Neoproterozoic age by Føyn and Glaessner (1979), as well as specimens from above the Ediacara Member in South Australia (Jensen et al., 1998), are regarded as early Cambrian in age. Kullingia specimens previously noted by McIlroy et al. (1997) and figured here (Fig. 4k and l) are consistent with an early Cambrian age.

3. Materials and methods

Samples collected by NBM are registered with the Australian Museum in Sydney as AMF125436–AMF125484. Specimens collected by DM are registered at Macquarie University, NSW as MU56152–MU56336. Seven additional samples from fragmental material are labelled A–F.

Wyeecha Spring was the main site for Ediacaran discoid fossil samples from uppermost Member II and lowermost Member III; the location was previously reported by McIlroy et al. (1997). Samples for petrography and sedimentary structures were also collected from Jinker Creek and Ellery Creek.

Thin sections cut the hyporelief surface containing discoid fossils and, wherever possible traversed the central boss of the discoid to investigate internal texture, sedimentary structure, and the presence or absence of a pyrite sole-veneer. Three thin sections were specifically cut as serial sections through a single high relief discoid fossil. In addition, thin section petrography examined host sediment texture, fabric and, most particularly, diagenetic history. Carbon coated rock chips were examined under a Jeol-733 SEM-microprobe for both fabric and mineralogy. Three samples were analysed on a Philips-EW1710 X-ray diffractometer to confirm grain and clay mineralogy.

4. Discoid morphology and sedimentation

4.1. The death-mask preservational model

Discoid fossils preserved in the Flinders-style (Narbonne, 2005) occur as moulds and casts on upper bedding surfaces or on lower bed soles (negative and positive epirelief or hyporelief, respectively) deposited as 'event beds' in siliciclastic sediments in shallow marine and deltaic environments. Surfaces bearing Ediacaran fossils commonly display irregular warty pustulose textures that Gehling (1987) compared with modern microbial mats, which was later invoked in the preservation of the fossils themselves (Narbonne, 1998; Gehling, 1999; Seilacher, 1999). Microbial mats represent communities of interwoven mucilaginous cyanobacteria and filamentous algae bound together as felted mats that make the substrate resistant to erosion in all but the strongest storms. Ediacaran fossils preserved in the Flinders-style are almost never found in beds lacking signs of microbial mats. A recognised suite of sedimentary structures provide evidence of former microbial mats (Hagadorn and Bottjer, 1997, 1999; Schieber, 1998, 1999), with wrinkle structure the principal identifier. Underlying wrinkle structures there are few grain-to-grain contacts, and sand-silt grains 'float' in dark clay-rich laminae (Noffke et al., 2002).

The taphonomic model proposed by Gehling (1999) to explain preservation of a soft-bodied biota in the Flinders-style preservation (Narbonne, 2005) implicates microbial mats as the critical binding and sealing mechanism during a late Neoproterozoic taphonomic window before the sea-bed was subjected to metazoan bioturbation and cropping during the Cambrian. Such mats are a necessary precondition for preserving moulds and casts of soft bodied organisms in sandstone. The hypothesis sees both mats and benthos smothered by sand during storms. Positive hyporelief casts were filled by sand from above after decay and collapse (cf. *Charniodiscus* in Gehling (1999, Fig. 11)). Conversely, negative hyporelief moulds were filled and cast from below by sediment from the substrate, and did not simply collapse, which necessitates the presence of a sole-veneer at the base of the storm-sand that was rigid enough to provide support before the organism entirely decayed (cf. *Dickinsonia* in Gehling (1999, Fig. 11)). Microbial re-colonization of the new sea-bed is inferred to seal the sediment-water interface, providing an anoxic micro-environment within the thin storm-sand. Hydrogen sulphide from bacterial decay (of the organism and microbial mat) and reduction of sea water sulphate is inferred to react with the abundant iron oxides present in the sediment to precipitate iron sulphide at the base of the sand immediately overlying the collapsed or resistant organisms, thereby forming an early diagenetic pyrite sole-veneer that acted as a 'death mask'.

4.2. Microbial mats

Wrinkle structure is common throughout the Arumbera Sandstone. For example, Type 1 wrinkle structure (Fig. 3a) is recorded in hyporelief in the uppermost Member II massive sandstone at Wyeecha Spring (wrinkle structure types from Bouougri and Porada, 2002). Type 2 wrinkle structure occurs in hyporelief on some cemented siltstone beds (Fig. 3b) in an otherwise hemipelagic-type mudstone section near the base of Member I about 1.8 km west of Ellery Creek. Microbial mats were thus ubiquitous on the Neoproterozoic seafloor within the Amadeus Basin.

4.3. Storm event beds

The cm- and dm-scale repetition of shale and siltstone in the lowermost Arumbera Sandstone Member I west of Ellery Creek attest to the periodic distal

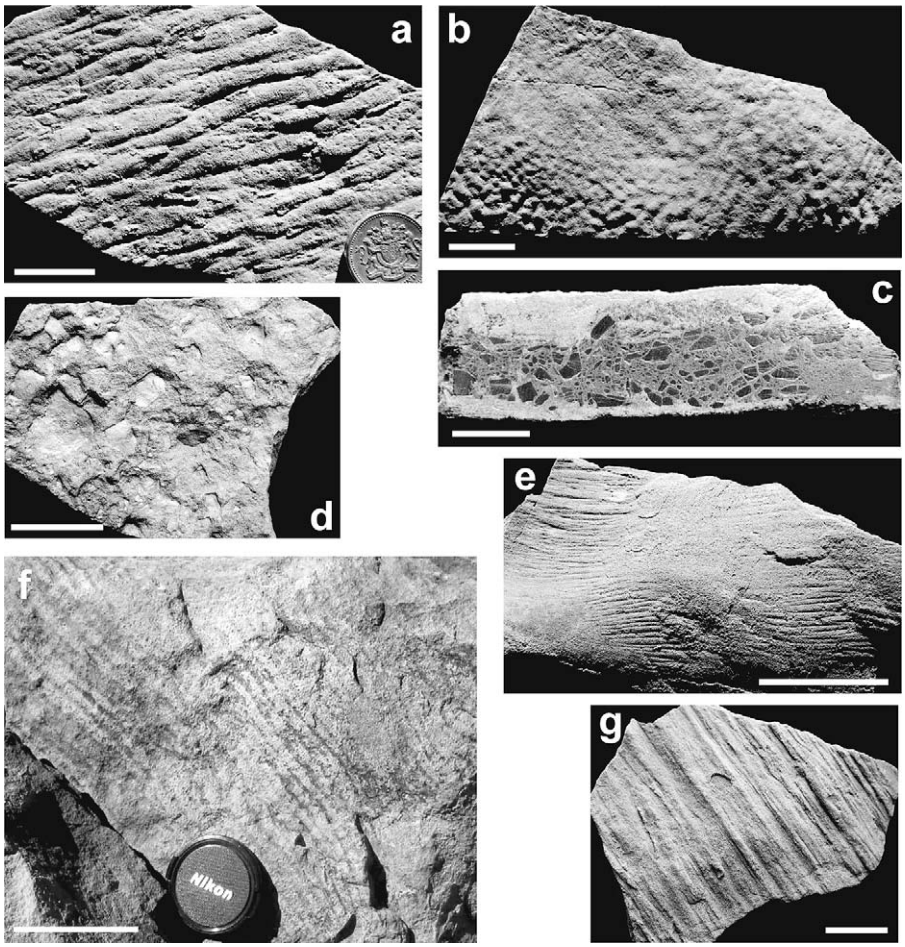

Fig. 3. Arumbera Sandstone sedimentary structures. (a) Type-1 wrinkle structure in hyporelief (AMF125439); (b) type-2 wrinkle structure in hyporelief (AMF125483); (c) mud-chip storm bed (AMF125484); (d) fine-grained sandstone–ironstone with angular mud chips (AMF125477); (e) pseudofossil Arumberia formed by storm currents acting on microbially bound surfaces with flute marks (AMF125443); (f) large pseudofossil Arumberia current structure; (g) groove marks in positive hyporelief confirm high storm-event current velocity (AMF125446). (a), (e) and (g) Wyeecha Spring, Member II; (b) and (c) 1.7 km west of Ellery Creek, Member I; (d) Jinker Creek, Member I; (f) 10 km east of Ellery Creek, Member II. Scale bars: all 2 cm, except (e) 5 cm and (f) 10 cm.

turbidite/tempestite depositional setting (Kennard et al., 1986). Less frequent yet stronger turbidity currents transported very-fine-grained sand that now form occasional hard bands. At this low level in Member I at Jinker Creek and at the equivalent lower levels in Member III at Wyeecha Spring (the fossiliferous horizon) similar periodic storm event flow applied.

Extreme storm bed deposits are inferred by the 1–4 cm thick mud-chip beds in Member I at both Ellery Creek west (Fig. 3c) and Jinker Creek (Fig. 3d). Angular thin chips up to 1 cm across testify to high-energy storm currents cascading down-slope, possibly sourced locally from rapid syn-depositional erosion.

Other structures indicative of high current flow include examples of pseudofossil Arumberia (Fig. 3e and f) and groove marks in positive hyporelief (Fig. 3g). The radially grooved Arumberia structure (the former cup-shaped fossil *Arumberia banksii* Glaessner and Walter, 1975) is common throughout the Arumbera Sandstone, and is re-described as a current generated flute-like structure on microbially bound sediment surfaces or matgrounds (McIlroy and Walter, 1997; McIlroy et al., 2005).

4.4. Discoid fossils

On the slope of a hillock 1.2 km NW of Wyeecha Spring [MP547516], 7 m above the Member II–III boundary, a fossiliferous horizon of abundant, but low diversity, discoidal fossils was discovered. The

succession is a series of cyclic inter-bedded dark-red shale, siltstone and very-fine to fine-grained sandstone. The sandstone beds (25–30 mm thick) display current ripples on upper bedding surfaces, internal ripple and fine parallel lamination, and an irregular base (the hyporelief fossiliferous surface). The uppermost very-fine-grained sandstone bed grades up into the overlying siltstone-shale. Patches of bedding-parallel trace fossils occur, but no vertical trace fossils were observed. The location is that reported by McIlroy et al. (1997 Fig. 10, midway between their Levels A and B).

The discoid fossils recorded from lowermost Member III at Wyeecha Spring (Fig. 4) are all preserved in positive hyporelief; the cast of their ventral surface. They range from 30 mm diameter low relief discoids (Fig. 4a) with marked peripheral rim and large central boss to small clustered <5 mm diameter flattened discoids (Fig. 4f). Others show relief up to 7 mm (Fig. 4b, c and h), some with fine concentric ornament. Discoids are either circular or slightly ovoid, others are significantly distorted (Fig. 4i and j) indicating structural deformation. Whatever their shape or size, all discoids have a characteristic central boss consisting of outer rim and central peak either protruding or recessed. Hand specimens exhibit a thin (<1 mm) dark-red clay-like coating on the hyporelief surface.

Approximately, 400 m NW of Wyeecha Spring a dry waterfall [MP552511] is formed by uppermost Member II massive and flaggy sandstone with granule trains. One fine-grained sandstone float sample yielded poorly preserved 8 mm diameter positive hyporelief discoid fossils with vague concentric structure (Fig. 4g).

Specimens of pseudofossil Kullingia previously recorded by McIlroy et al. (1997) from Arumbera Sandstone Member III at Wyeecha Spring and Valley Dam are figured here in Fig. 4k and l.

4.5. Discoid fossil affinity

Well preserved examples of the Ediacaran discoid fossil *Aspidella* from southeastern Newfoundland, originally described by Billings (1872), are shown to be highly variable in morphology (Gehling et al., 2000). The eventual shape and ornament of the fossilised holdfast bulb is dependent upon the thickness and order of sand and clay lamination involved during burial. They conclude that these discoid fossils are holdfasts of frond-like organisms and define an intergrading plexus of morphs with three end-member 'form-genera' that represent different preservation states of the same fossil. Their interpretation of *Aspidella* implies that all its morphs are a single taxon, and many Ediacaran discoid taxa described over the last 50 years are junior synonyms of *Aspidella*, including the common species *Ediacaria*, *Cyclomedusa*, and *Spriggia*.

Most of the Arumbera Sandstone discoid fossils presented in Fig. 4 are simple morphological forms that are assigned to the *Aspidella* plexus. Discoids shown in Fig. 4b and c and h are probably representatives of the convex *Ediacaria* form-genus, with Fig. 4f as small examples and those in Fig. 4i and j distorted examples. Discoids in Fig. 4a and d from the same horizon show affinities closer to the flat *Spriggia* form-genus. In contrast, the small globular discoids from uppermost Member II (Fig. 4g) show greater affinity to the genus *Beltanelliformis* (see review in McIlroy et al., 2005).

4.6. Thin sections through discoids

Thin sections through fossils reveal fine internal lamination and sedimentary structures (Fig. 5). The first striking feature is the wide-V form of the discoid's hyporelief surface. Also noted is the red-brown coating retained intermittently along both the hyporelief and epirelief surfaces (solid black ornament on sketches), and well seen in Fig. 5a and e. It occurs intermittently as an even thinner coating on other hyporelief surfaces (dotted ornament) with a thickness little more than sand grain size. This red-brown coating is that previously noted from hand specimens. Photomicrographs (Fig. 6a–d) illustrate at higher magnification a matted texture of clay, haematite and some fine silt, that is present as a superficial coating to the fossil surface (Fig. 6a and b) or interbedded within the fine laminations (Fig. 6c and d). The upper and lower margins of the veneer are compressed against surface irregularities, and do not penetrate deep into sand interstices. It is interpreted as a diagenetic artefact of the original microbial mat.

Fine internal lamination is well developed and preserved at two scales. Firstly, sub-horizontal, bedding-parallel, pale sandstone laminae alternate with red-brown clay-haematite rich laminae. These laminations are continuous across the section and are represented on the sketches by solid lines (Fig. 5). Secondly, ripple cross-laminae are emphasised in all three serial sections (Fig. 5a–c), with acute rather than asymptotic basal contact. The cross-laminae are illustrated by broken lines in the sketches. Bedding-parallel laminations represent individual sediment flows within a storm event, which were overgrown by an epirelief microbial mat when conditions calmed after the storm. The cross-laminae are current ripple foresets formed above the hyporelief microbial mat.

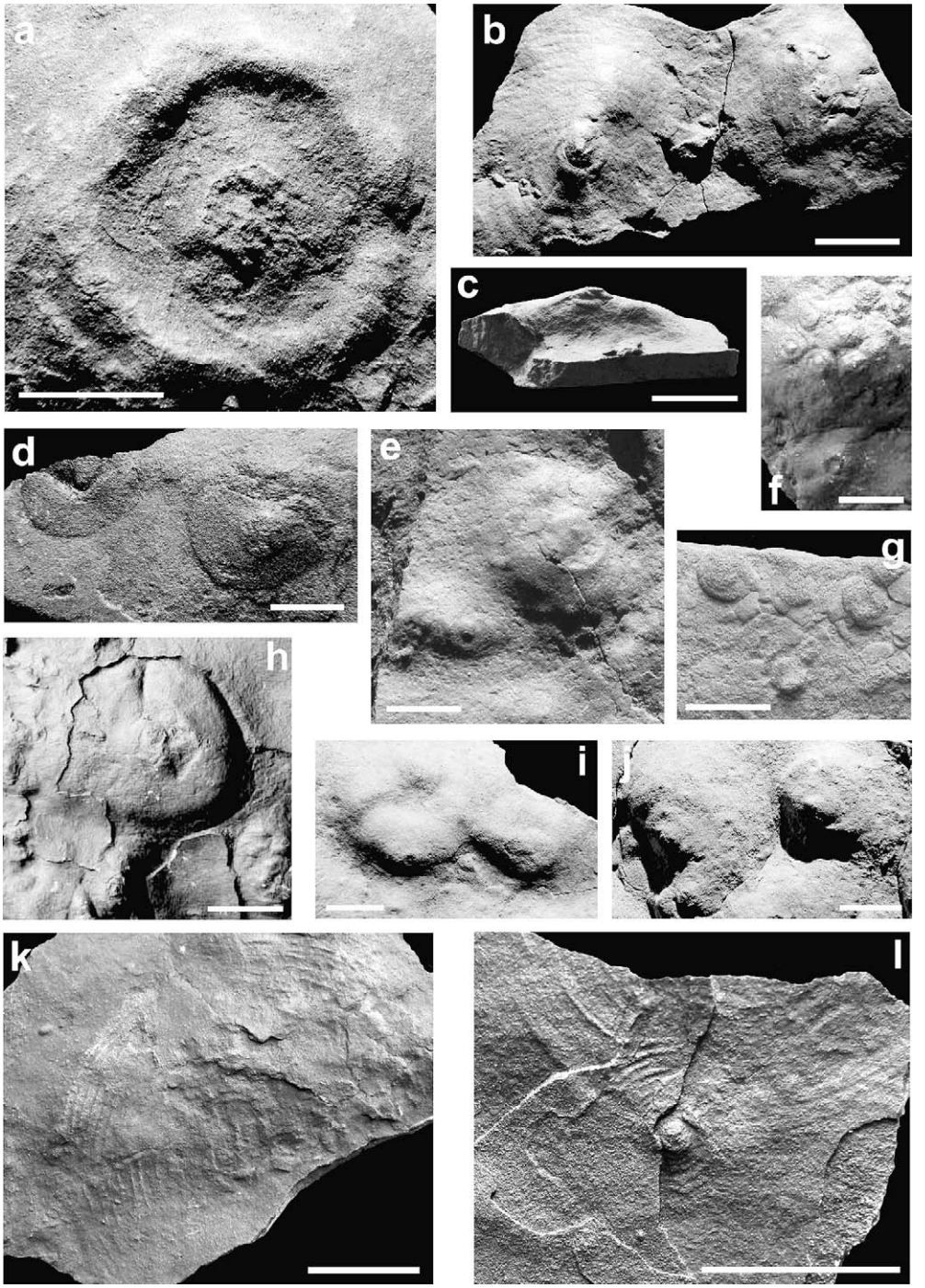

Fig. 4. Arumbera Sandstone discoid fossils (a–j) and pseudofossils (k–l). (a) Low relief discoid with pronounced peripheral rim and central boss (MU56325); (b) and (c) high relief discoid, as shown by side view of (b) in (c), with protruding central boss and distinct fine concentric ornament (sample F); (d) flat discoids lacking raised peripheral rim (MU56306); (e) slightly distorted discoids with protruding central boss (AMF125469); (f) clustered small discoids with prominent central boss; larger discoid below (MU56296); (g) high relief discoids with vague concentric ornament (AMF125440); (h) high relief discoid with smaller discoids below (sample E); (i) deformed discoids with recessed central boss (AMF125462); (j) deformed discoids with protruding central boss and hint of concentric ornament (AMF125465); (k) Kullingia wave-induced scratch circle—from just below Level C in McIlroy et al. (1997, Fig. 10) (MU56262); (l) two superimposed Kullingia scratch circles, the smaller formed on adjacent bedding lamination <1 mm thick—from just below Level D in McIlroy et al. (1997, Fig. 8) (MU56336). All Wyeecha Spring except (l) Valley Dam. All Member III except (g) Member II. Scale bars: all 1 cm. No retro-deformation performed.

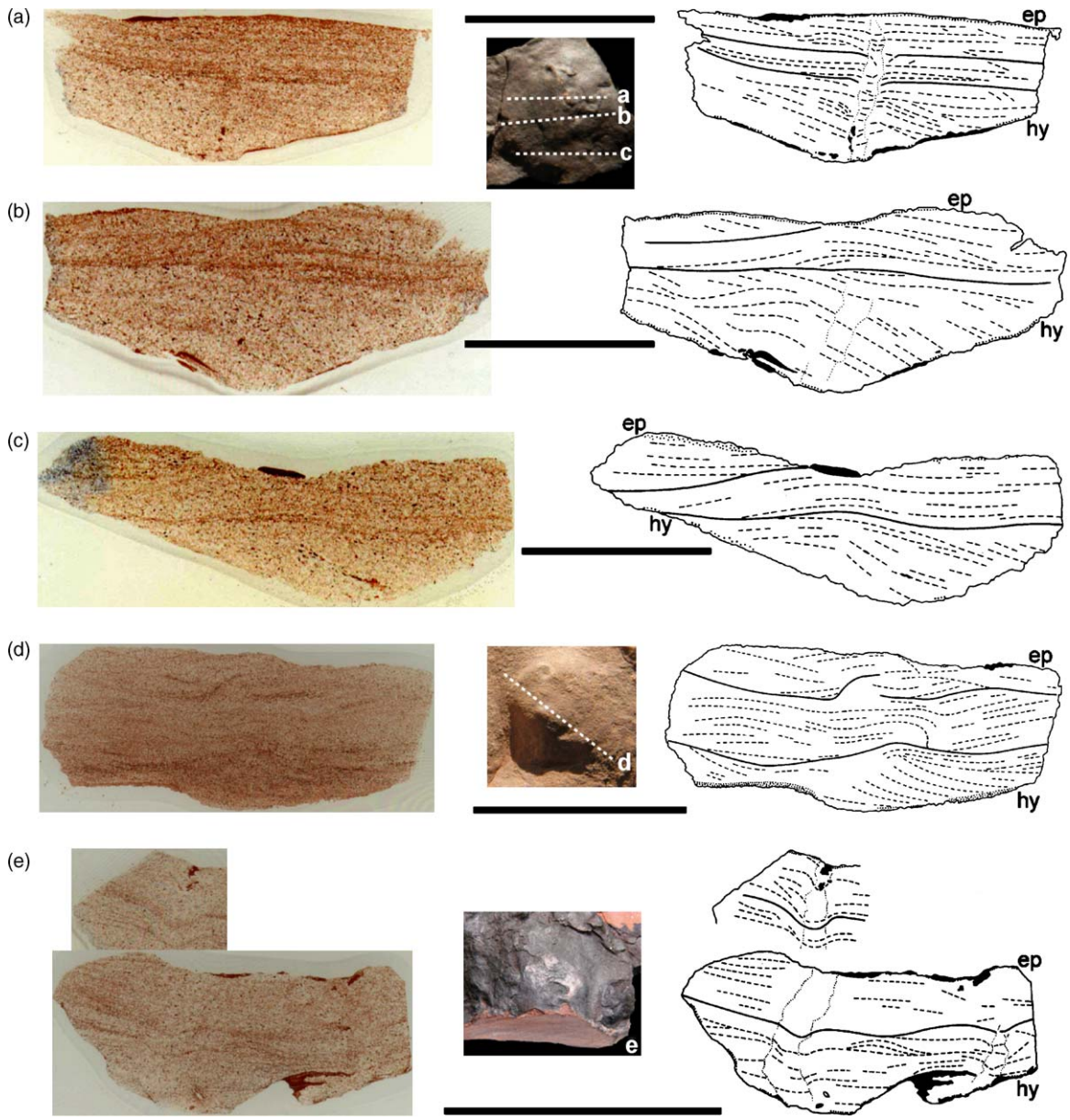

Fig. 5. Thin sections through discoid fossils with sketches. (a)–(c) Serial thin-sections through high relief discoid; inset shows hyporelief view with location of thin sections (a–c) (sample F; see right side of Fig. 4b); (d) flattened discoid with well developed basal cross-laminae; insert shows hyporelief view with location of thin section (d) (AMF125465; see right side of Fig. 4j); (e) two closely spaced slices through high relief discoid; insert shows hyporelief view with cut surface for thin section (e) (sample E; discoid located 7 cm from Fig. 4h). Note hyporelief (hy) and epirelief (ep) clay/haematite coating (solid black ornament where well developed, dotted where thin), bedding-parallel lamination (solid line) and current-ripple cross-laminae (broken line), and sub-vertical zone of disturbance where laminae arc downwards in (a), (b) and (e). All Wyeecha Spring, Member III. Bar scales: 20 mm.

In several thin sections (Fig. 5a, b and e) a sub-vertical zone of disturbed laminae extends, without change in width, from the area of the discoid's central boss (the lowest point of the V-form) upward to the epirelief clay-haematite veneer. Fine internal laminae arc downwards within this disturbed zone (Figs.5a and e and 6e).

4.7. Sequence of burial events

A sequence of sedimentary events during holdfast burial is evident from the studied sections and presented step-by-step in Fig. 7. A mucilaginous microbial mat formed on the Neoproterozoic sea-bed during a quies-

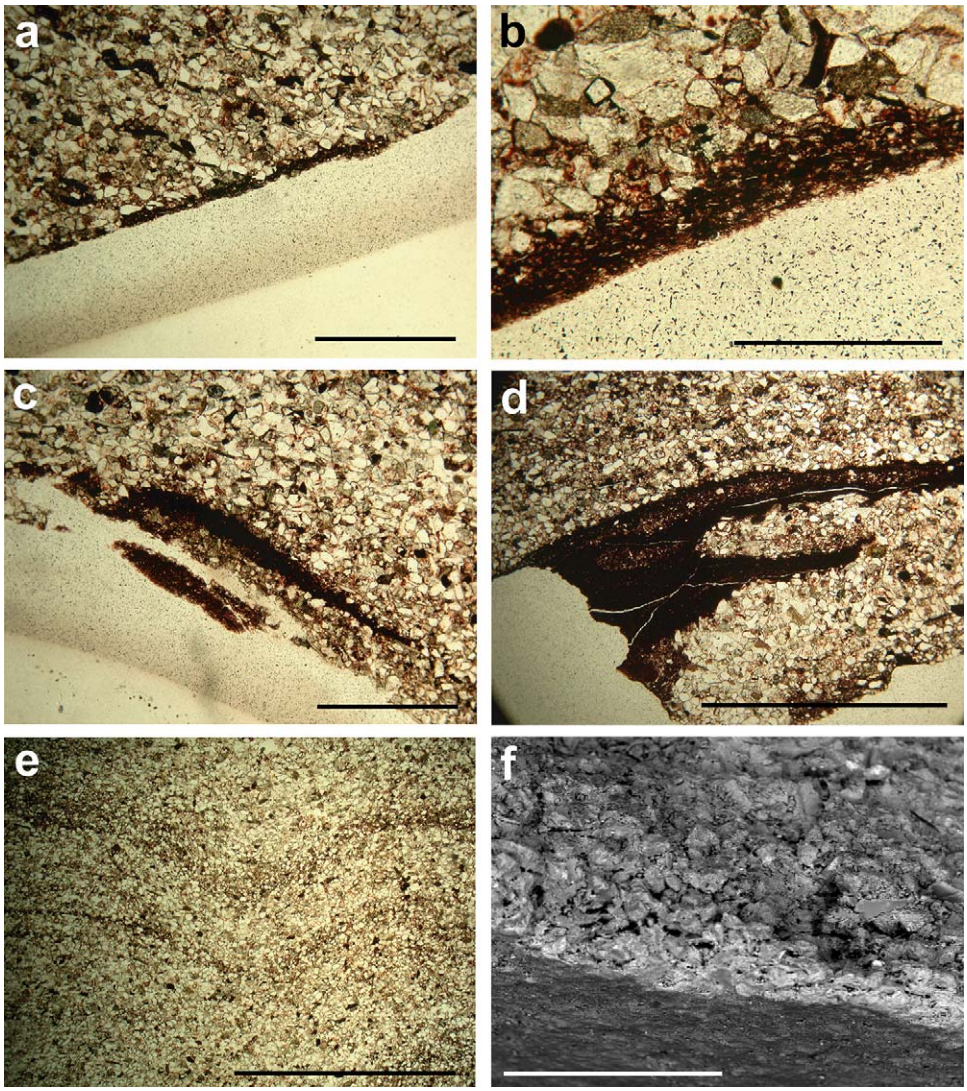

Fig. 6. Photomicrographs of clay/haematite coating on hyporelief surface of discoids shown in Fig. 5; displays mixture of clay and haematite with some fine silt. (a) Lower right of Fig. 5b; (b) lower right of Fig. 5a; (c) lower right of Fig. 5e with interlaminated pinched out clay/haematite coating; (d) lower left of Fig. 5b with double clay/haematite layer; (e) bedding-parallel lamination arcs downwards in the sub-vertical zone of disturbed lamination shown in Fig. 5e; (f) SEM of siltstone with marked edge-effect along hyporelief surface; no pyrite or clay/haematite detected. All Wyeecha Spring, Member III. (a), (b) and (d) sample F; (c) and (e) sample E; (f) AMF125469. Bar scales: (a), (c) and (d) 2 mm; (b) 1 mm; (e) 4 mm; (f) 500 μm.

cent period and the holdfast-bulb of a frondose-stalked organism attached itself to the microbial mat (Fig. 7a); probably at least partially embedded within, rather than stuck onto, the microbial mat. It is likely the frondose organism filter fed through its frond during current movement. Modest current flow induced the formation of small current ripples that lapped over and around the holdfast-bulb and stalk, but the organism continued to feed (Fig. 7b). A major storm event, or several events, engulfed the stalk and bulb, the force of which snapped off the frond and the organism, being unable to regenerate, died. The holdfast-bulb decomposed quickly (before the more rigid tough flexible stalk) or simply collapsed so microbial mat, ripple foresets and remaining stalk sank into the vacant bulb cavity (Fig. 7c). Quiet conditions returned after the storm, the stalk eventually decomposed and internal ripple and bedding lamination arced downwards into the stalk cavity (Fig. 6e). A new microbial mat developed over the seabed during this later quiescent period (Fig. 7d), and restricted the free flow of oxygenated waters through the storm sand so anaerobic conditions formed as a micro-environment between the

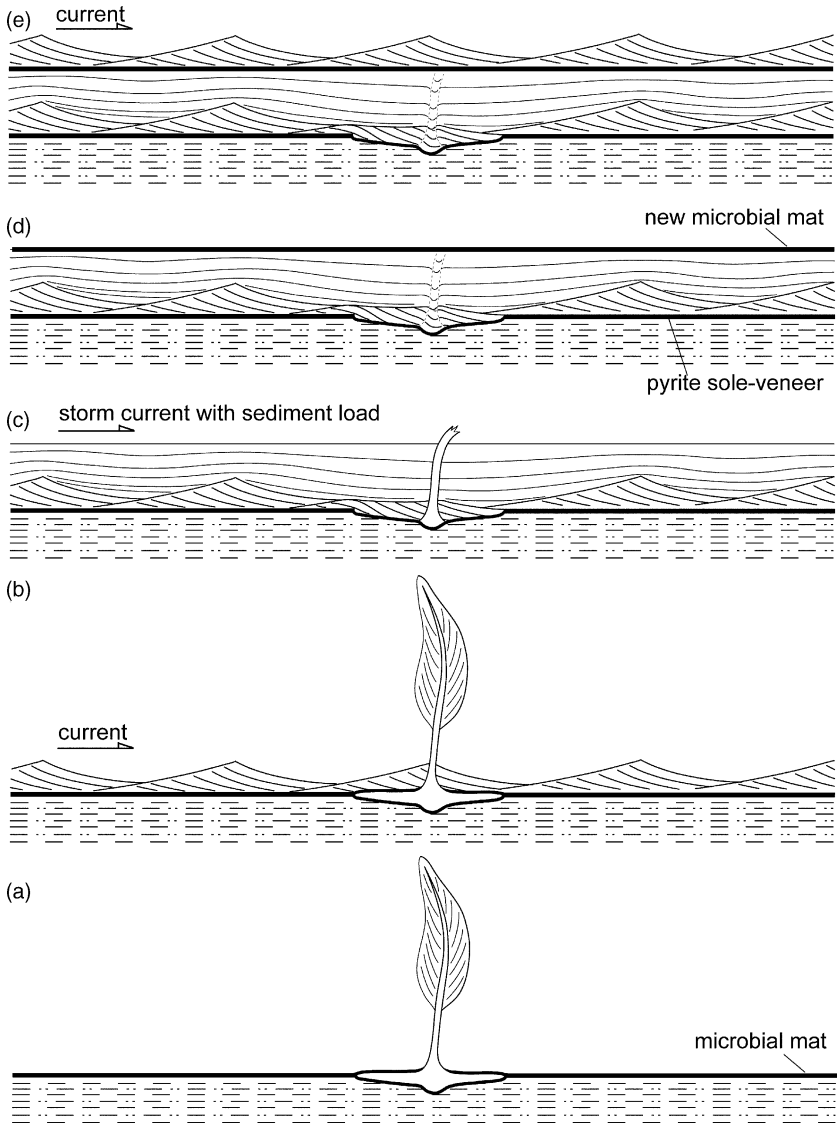

Fig. 7. Burial sequence for organism composed of frond, stem and holdfast-bulb. (a) Mucilagenous microbial mat formed on the sea bed during quiescent period and holdfast-bulb stuck to or embedded in microbial mat; frond filter fed from current; (b) current flow formed small current-ripples that lapped over holdfast-bulb, but the organism continued to filter feed; (c) major storm event, or several events, engulfed stem and bulb; frond broke away so organism died; bulb decomposed and collapsed before stem, microbial mat and ripple sank into vacant bulb cavity with reduced foreset angle, but increased basal contact angle; (d) storm long ceased, stem decomposed and storm bed laminations locally sank into vacant stem cavity; new microbial mat formed; early diagenetic pyrite formed a sole-veneer in an anaerobic micro-environment between the two microbial mats; (e) re-newed current ripples. Not to scale.

two mats. Early eodiagenetic (syn-depositional) pyrite developed as a sole-veneer at the contact of sediment with the lower microbial mat (perhaps even replacing filaments of the microbial mat) and thus provided the vital rigidity for fossil preservation. New current ripples would have eventually formed above the new microbial mat (Fig. 7e). The sub-vertical zone cross-cutting bedding laminations and ripple cross laminae is interpreted as the former position of the frondose organism's stalk, an interpretation not previously proffered. Fine bedding and ripple laminae arc downwards into this disturbed zone to fill the space vacated by the decayed stalk.

4.8. Pyrite sole-veneer

A thorough SEM search for framboidal pyrite (or iron oxide pseudomorphs) along the fossiliferous hyporelief surfaces in the present Arumbera Sandstone samples,

provides no direct evidence for a pyrite sole-veneer. Similarly, Gehling (1999) acknowledges there is no direct evidence of a pyrite sole-veneer at the South Australian localities. The <1 mm clay-haematite coating on hyporelief surfaces in hand specimen and thin section (Fig. 5a–d) is here interpreted as clay and fine silt 'raining' out of suspension onto the sticky microbial mat during prolonged fair weather periods between storms. This provided considerable mechanical resistance in its own right, probably sufficient to retain embedded holdfasts while their exposed fronds were swept away by sand-laden storm currents.

The sole-veneer initially precipitated as an iron monosulphide precursor FeS at the contact of the sand immediately overlying the collapsed (positive hyporelief) or resistant (negative hyporelief) decaying organisms and the mat surface. However, the monosulphide precursor is metastable and transforms to pyrite FeS_2 (see eodiagenetic summary below). Pyrite is stable under anoxic low temperature sulphidic conditions (Berner, 1981) with pH range neutral to alkaline and low carbonate activity (see Eh-pH stability diagram for the Fe–O–H–S system in Ottonello (1997, Fig. 8.22C)). It has been shown experimentally that pyrite formation is confined to a zone directly adjacent to the organic matter (Allen, 2002).

Many examples of soft bodied animal and plant fossilisation via replacement framboidal pyrite are known from Phanerozoic mudstone lagerstätten (Devonian Hunsrück Slate, Briggs et al., 1996; Eocene London Clay, Grimes et al., 2002). Moreover, direct evidence for a Neoproterozoic pyrite sole-veneer is recorded from the White Sea, where a thin (<1 mm) hyporelief impregnation of framboidal pyrite within the basal sand grains in the vicinity of fossils is retained through to the present (Dzik, 2003). Freshly quarried samples are covered in pyrite, which readily oxidises upon exposure. No pyrite is recorded from within the mat itself, only clay minerals. The elusive sole-veneer, therefore, formed above the microbial mat within the lowermost few sand grains of the event sand. The unidentifiable rind-like effect visible along the hyporelief surface in one present sample under SEM (Fig. 6f) is clearly indicative of some form of interstitial cementation within a <1 mm surface zone.

At this stage in the death mask model, however, Gehling simply states that '*later. . .. . .pore-water flushing*' (1999 p. 53) eventually oxidised the pyrite sole-veneer to haematite. The remainder of the present paper traces the diagenetic trail from the inferred pyrite sole-veneer to the thin haematite coating seen today in the Arumbera Sandstone of the Ooraminna Sub-basin.

5. Diagenetic history

5.1. Petrography

The Arumbera Sandstone is mainly a subarkose with some arkose and sublith-arenite (granule) horizons. Quartz accounts for 75–84% of detrital grains in sandstone (48–63% monocrystalline, 17–27% polycrystalline), feldspar 8–14% (5–10% orthoclase, 1–6% microcline, 1–3% plagioclase), and lithic rock fragments 7–16% (mainly microcrystalline chert). Siltstone greywacke (>15% matrix) shows greater variability with 72–92% quartz, 6–23% feldspar and 2–5% lithic rock fragments. Authigenic quartz overgrowths generally account for 7–11% of the rock volume, whilst authigenic feldspar is present in minor amounts. Porosity varies from 0 to 9%. Carbonate accounts for 1–3% of sandstone, but 32% in some siltstone.

5.2. Sandstone texture and fabric

Member I siltstone to fine-grained subarkosic sandstone is poor to moderately sorted with sub-angular to sub-rounded detrital grains (Fig. 8a–d). Member II is mainly immature, very-fine to medium-grained, poorly to well sorted, sub-angular to sub-rounded subarkosic sandstone (Fig. 8e–h). Very-coarse-grained sublitharenite beds contain either granule trains or basal granule beds. Member III siltstone and sandstone (Fig. 8i and j) is texturally similar to Member I.

Detrital grains exhibit iron-oxide stained clay rims, except at grain-to-grain contacts where only a thin 'dustline' marks the detrital grain margin (Fig. 8c and d). Clay rims are ubiquitous and clearly authigenic. Authigenic quartz overgrowths vary from anhedral pore fill with irregular sutures to subhedral crystal faces in open pores. Authigenic quartz clearly post-dates the authigenic clay rims. Where authigenic quartz and feldspar overgrowths occur together, the feldspar often exhibits its subhedral tooth-like growth form while the quartz overgrowth fills in the remaining vacant pore space (Fig. 8g and h); authigenic feldspar preceded authigenic quartz. Glauconite peloids occur in Member III (Fig. 8i and j).

Member III siltstone and sandstone contains considerable dolomite, as patchy irregular semi-poikilotopic pore fill (Fig. 8i and j). The aggressive dolomite replacement 'front' partially or totally replaces detrital grains, leaving a 'ghost' clay rim outline of the former detrital grain. Staining with Alizarin Red S followed by potassium ferricyanide confirms non-ferroan dolomite.

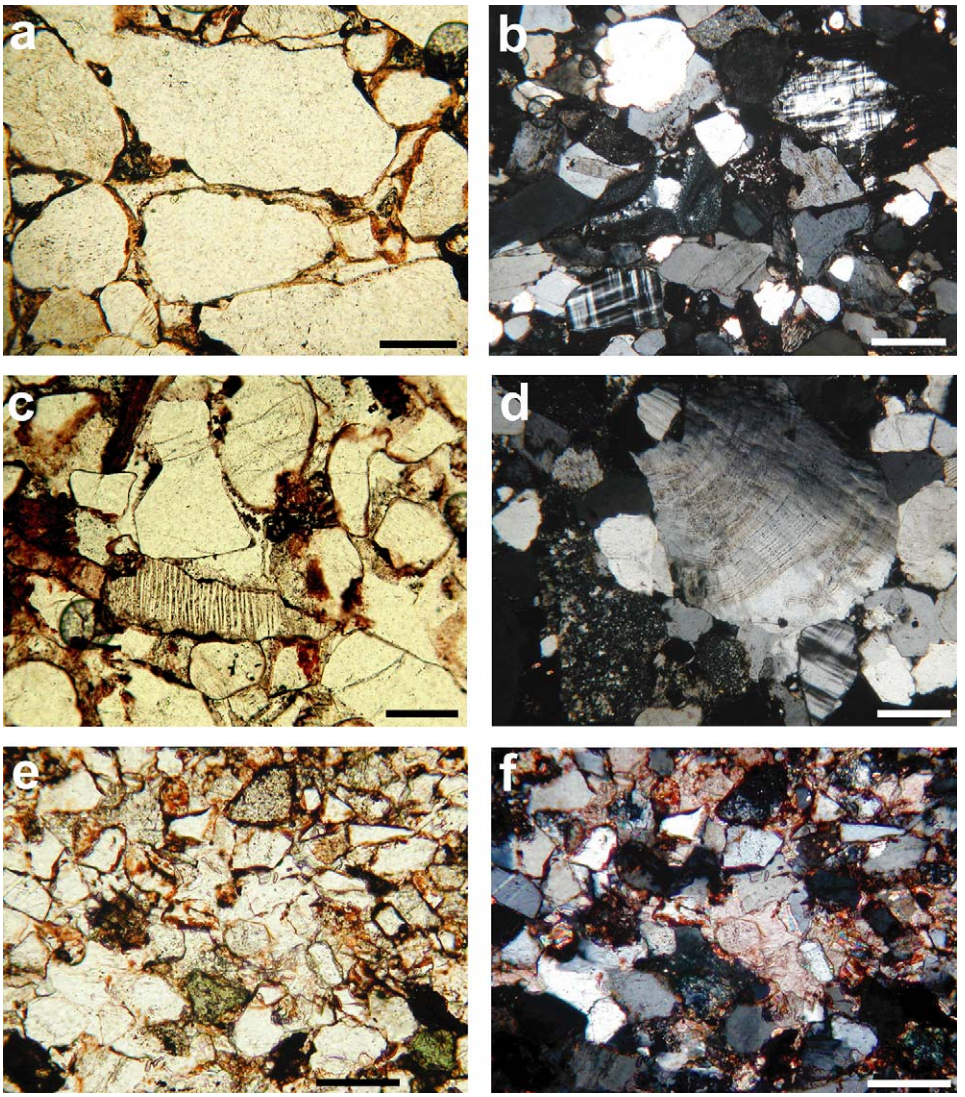

Fig. 8. Arumbera Sandstone photomicrographs. (a) PPL; marked authigenic clay rims, except at grain-to-grain contacts where only thin dust-line; authigenic quartz overgrowths (AMF125454); (b) XPL; high feldspar content; detrital grain of former silicified ooid (centre left) (AMF125454); (c) PPL; elongate perthitic feldspar with subhedral tooth-like authigenic overgrowth that post-dates the authigenic clay rims but pre-dates the authigenic quartz pore filling (AMF125450); (d) XPL; granules of microcrystalline chert (lower left) and silicified stromatolite (centre) (AMF125476); (e) and (f) PPL and XPL; glauconite grains (lower centre and lower right); irregular patches of poikilotopic pore filling dolomite corrodes, replaces and engulfs adjacent detrital quartz grains leaving clay rim 'ghosts' (centre right); dolomite post-dates authigenic quartz (AMF125467). (a), (b) and (d) Jinker Creek; (c), (e) and (f) Wyeecha Spring; (a) and (b) Member I; (c) and (d) Member II; (e) and (f) Member III. Scale bars: (a), (c) and (d) 0.1 mm; (b), (e) and (f) 0.05 mm.

5.3. SEM/microprobe analyses

Authigenic quartz (Fig. 9a centre right) partially surrounds its well-rounded detrital parent (upper centre), but its complete envelopment of the detrital grain is inhibited by earlier authigenic K-feldspar (left with blocky cleavage) abutting the detrital quartz grain. In addition, rare albite grains indicate some measure of albitization of plagioclase feldspar.

Both detrital and authigenic illite are represented, the latter with characteristic flaky and filamentous habit (Fig. 9d), where ribbon-like filaments bridge pore throats. No kaolinite was seen in SEM despite an extensive search. Thin subhedral pseudohexagonal platelets of chlorite replace occasional detrital grains (Fig. 9g). The third clay mineral is smectite, which is well developed in its classic crenulated webby pore-lining habit (Fig. 9e and h). No smectite occurs across the scars marking for-

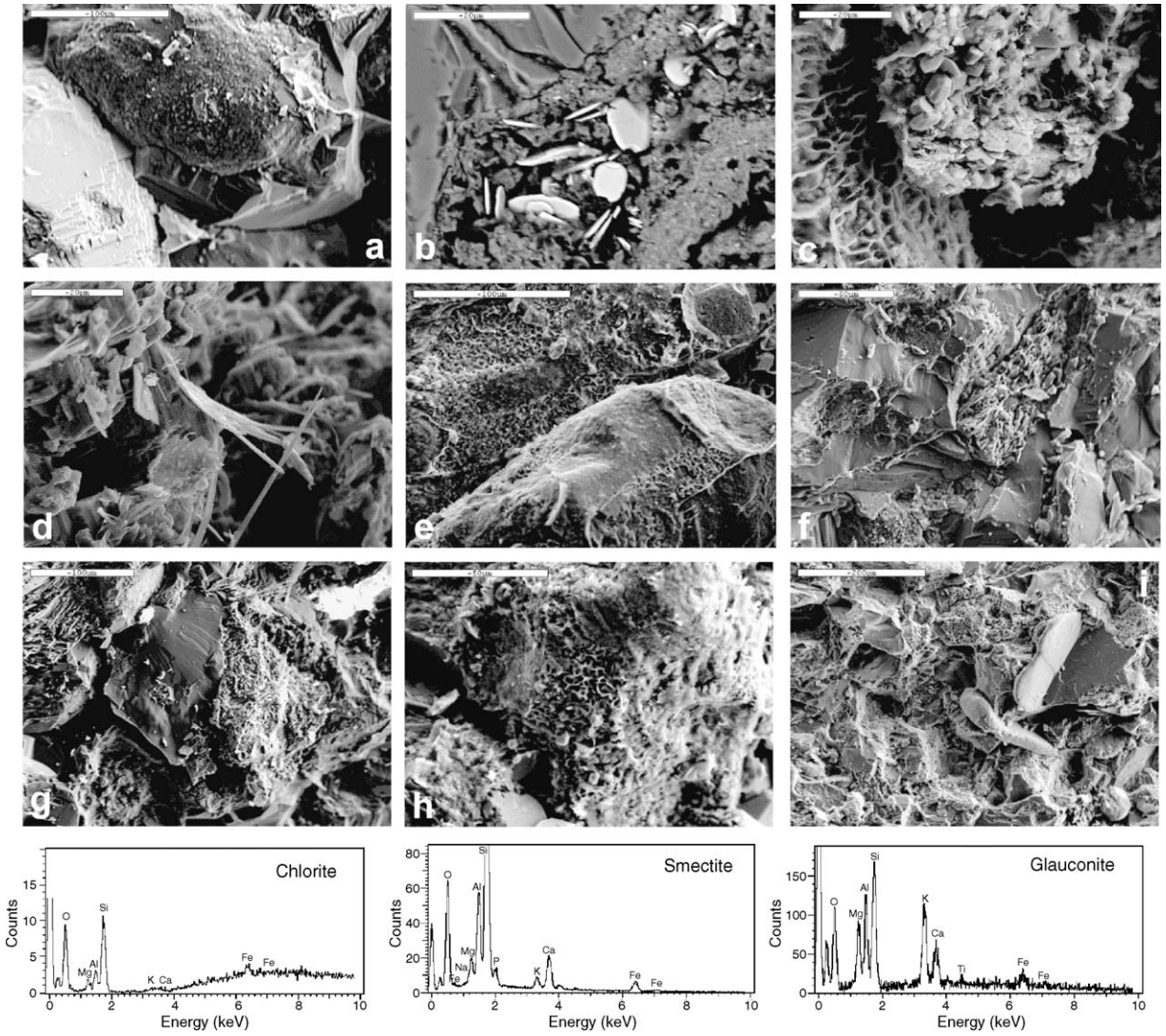

Fig. 9. SEM micrographs-microprobe spectra. (a) Well-rounded quartz grain with enveloping authigenic quartz overgrowth (right centre) and authigenic K-feldspar (left); authigenic K-feldspar pre-dates authigenic quartz; (b) discus-shaped platelets of authigenic haematite (centre) set centrally within clay matrix; (c) thin blocky platelets of authigenic haematite (centre) as pore-filling that post-dates webby smectite rim on detrital grain (left); (d) flaky authigenic pore-filling illite (left) and filamentous pore-bridging illite (centre); (e) crenulate webby texture of rim forming smectite; grain contact scars confirm smectite as authigenic; (f) fractured glauconite peloid (centre) shows internal flaky microtexture; (g) grain replacing platelets of authigenic chlorite; spectrum shows typical chlorite elements Si, Al, Mg, Fe and Ca; (h) thin webby crust of authigenic smectite coating detrital grains; spectrum shows typical elements of smectite Si, Al, Ca, Mg, Fe and K. (i) rounded and flattened glauconite peloids; spectrum shows typical elements of glauconite Si, Al, Mg, K, Ca, Fe and Ti. All Wyeecha Spring except (d) and (e) Jinker Creek. All Member II except (b) and (i) Member III; (a), (f) and (g) AMF125473; (b) and (i) AMF125469; (c) and (h) AMF125450; (d) and (e) AMF125453. Scale bars in μm.

mer grain-to-grain contacts (Fig. 9e centre right). The smectite is thus authigenic, and the first pore-lining clay formed immediately upon the dust-line.

Haematite occurs as thin, very small (5 μm diameter) discus-shaped crystals (Fig. 9b and c). The haematite is pore-filling and occupies a central, therefore late, position within pores, and clearly post-dates the webby smectite pore-lining (Fig. 9c left). Flattened well-rounded peloids of glauconite occur (Fig. 9i centre right) composed of irregular glauconite platelets (Fig. 9f centre right).

5.4. X-ray diffraction analyses

XRD analyses confirm the main detrital grains and dolomite cement (Fig. 10). Air dried (including glycol)

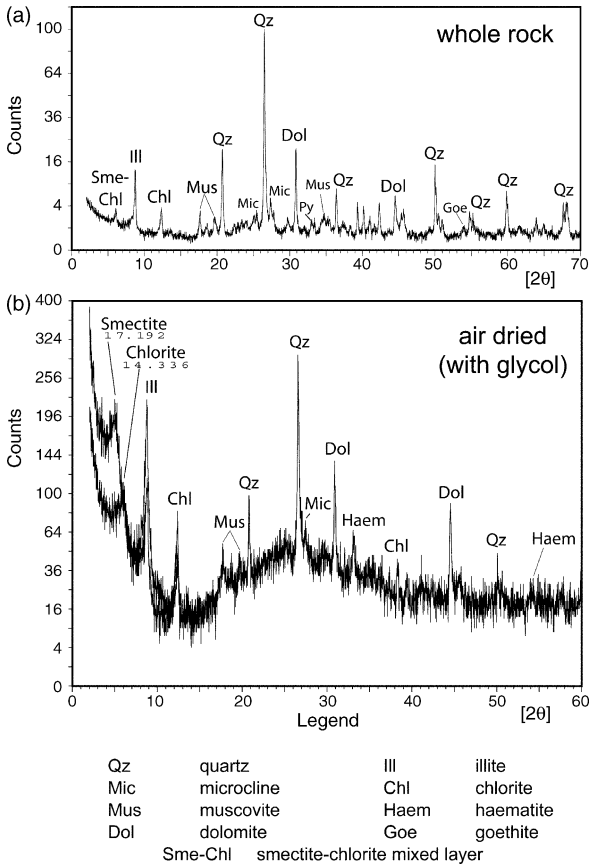

Fig. 10. XRD summary spectra. (a) Whole rock; (b) air dried <2 μm fraction with glycol. Wyeecha Spring, Member III, AMF125471.

analyses demonstrate chlorite peaks, particularly that at $2\theta = 12.3°$. The strong peak at $2\theta = c.8.8°$ (Fig. 10b) confirms the 10 Å basal spacing of illite, while a broad peak at $2\theta = c.6°$ identifies a smectite–chlorite mixed-layered clay. The presence of the iron-oxide haematite is confirmed (Fig. 10b), with a trace of goethite in the whole rock analysis (Fig. 10a).

5.5. Basin subsidence history

Published tectonic-subsidence curves (Lindsay et al., 1987; Lindsay and Korsch, 1991), taken together with overall basin structure and stratigraphy (Walter and Veevers, 2000; Veevers, 2000), particularly through the Palaeozoic, provide a snapshot view of basin subsidence which in turn puts a broad relative time frame to diagenetic events. The Arumbera Sandstone experienced continuous basin subsidence and burial through the Cambro-Ordovician to its deepest burial during the late Ordovician (3–4 km). In the north-eastern Amadeus Basin, Rodingan regional uplift and tilting resulted in Silurian erosion of up to 3000 m of section (Wells et al., 1970; Lindsay and Korsch, 1991) with 'molasse' sedimentation through to the Devonian. Central Australia experienced a long 300 Ma period of subaerial telogenesis as the Arumbera Sandstone followed an extended climb back to the present weathering surface, a feature relevant to Ediacaran fossil preservation.

5.6. Eodiagenesis and formation of the pyrite sole-veneer

Petrographic analyses provide evidence to generate a sequence of diagenetic events (Fig. 11). Arumbera Sandstone diagenetic history commenced with the (syn-depositional) formation of a pyrite sole-veneer and a subsequent trail of anoxic and later oxic events leading to the haematite seen today.

Much research into early diagenetic pyrite formation is available in the specialised geochemical literature (Canfield and Raiswell, 1991; Schoonen and Barnes, 1991; Berner, 1994; Wilkin and Barnes, 1997; Canfield et al., 1998; Butler and Rickard, 2000; Grimes et al., 2001; Schoonen, 2004), though the actual mechanism of iron disulphide growth under sedimentary conditions is still elusive, and reaction rates in field studies are slower than in laboratory experiments (Schoonen, 2004). Under anoxic conditions, hydrogen sulphide is produced via the biologically mediated sulphate reduction of organic compounds in the presence of dissolved pore-water sulphate (Fig. 11, Eq. (1)). Hydrogen sulphide then reacts with iron minerals in the sediment to produce an iron monosulphide precursor (either amorphous FeS or poorly crystalline mackinawite FeS) and elemental sulphur (Fig. 11, Eq. (2)). Rickard (1995) and Herbert et al. (1998) report that experimentally an initial amorphous mackinawite precipitates after two days at 25 °C, whilst mackinawite crystallisation may take tens to hundreds of days to develop, and complete well-crystallised mackinawite requires up to two years at 25 °C. Some researchers argue that elemental sulphur then oxidises mackinawite to a second precursor greigite, and eventually to pyrite (Sweeney and Kaplin, 1973; Wilkin and Barnes, 1997) (Fig. 11, Eq. (3)), whereas Butler and Rickard (2000) dispute the necessity for greigite as a prerequisite for framboidal pyrite formation, and demonstrate experimentally that only the monosulphide mackinawite acts as a precursor.

In experimental work with pure and field-sample bacteria cultures Canfield et al. (1998) forward two alternative competing pathways for the conversion of FeS to pyrite. Either elemental sulphur oxidises FeS directly to pyrite (Fig. 11, Eq. (4)), or the abundant bacterially gen-

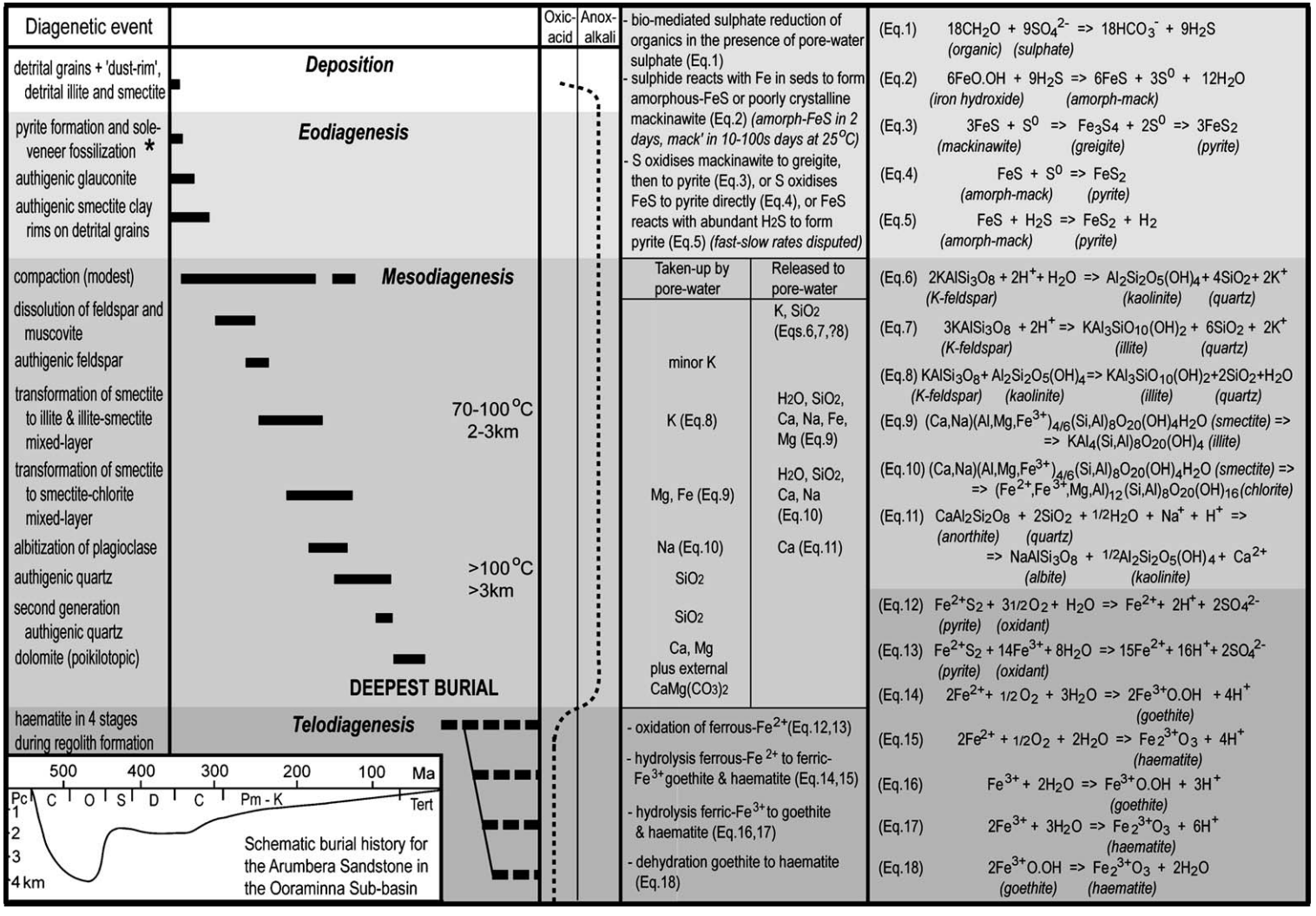

Fig. 11. Sequence of diagenetic events for the Arumbera Sandstone, illustrating the standard sub-division into eodiagenesis (early - light grey), mesodiagenesis (burial - medium grey) and telodiagenesis (uplift - darkest grey), a schematic burial curve, and main pore-water reactions. After deposition, pore-waters remained anoxic and neutral-mildly alkaline through eo- and mesodiagenesis and deepest burial, changing to oxic-mildly acid due to meteoritic water flushing through the deep regolith during telodiagenesis. Asterisk indicates near syn-depositional event. All time implications are relative. Eqs. (1)–(3) derived from Canfield and Raiswell (1991), (4) and (5) after Schoonen (2004), (6)–(8) after Worden and Morad (2000), (9) and (10) after Pettijohn et al. (1987), (11) after Morad et al. (2000), (12) and (13) after Loope and Watkins (1989) and Rimstidt and Vaughan (2003), (14) and (15) after Loope and Watkins (1989) and Cornell and Schwertmann (1996), and (16)–(18) after Cornell and Schwertmann (1996).

erated hydrogen sulphide present in anoxic sediments oxidises the sulphur in FeS to yield pyrite with hydrogen as the reduced product (Fig. 11, Eq. (5)). They conclude that these reactions operate either separately or simultaneously, with measured reaction rates equally fast and considerably faster than expected from inorganic reactions, so bacteria may enhance rates of pyrite formation in natural systems. However, the high conversion rate proposed by Canfield et al. (1998) is considered inconsistent with field observations by Schoonen (2004) who interprets the H_2S conversion rate to be slow in the order of decades to centuries. Furthermore, Canfield and Raiswell (1991) observe that as pyrite framboids can be produced synthetically through inorganic reactions, the critical biogenic role is in producing the hydrogen sulphide. It is also argued that biogenic cell walls also help promote the nucleation of initial pyrite, after which the rate of pyrite formation was enhanced (Schoonen, 2004).

Glauconite (Figs.8e and f, and 9f and i) forms through recrystallization of smectite during eodiagenesis in shallow marine environments with low sedimentation rates, and associated organic matter creating local reducing conditions (Tucker, 2001), often associated with early pyrite. The presence of glauconite in the Arumbera Sandstone fossiliferous horizons confirms that pore-waters remained reducing and neutral-alkaline during burial, so the pyrite sole-veneer remained intact through eodiagenesis.

Substantial webby smectite clay rims surround most detrital grains, except at grain-to-grain contacts (Fig. 9e), demonstrating that the rim smectite is authigenic and eogenetic. The source of authigenic grain rimming smectite is uncertain, and could be biogenic (Needham et al., 2005). The early transformation of original detrital smectite to authigenic rim smectite is a likely possibility. Alternatively, smectite could be transformed from the devitrification of volcanic glass (Pettijohn et al., 1987) whereupon Na^+, Ca^{2+} and some K^+ are released into the pore-water. Mafic lavas and dolerite dykes of the Petermann Ranges are a potential source of such material.

5.7. Mesodiagenesis

Temperature, pore-water composition and residence time are the main controls on mesodiagenesis. Two diagenetic sub-divisions are in common usage (Morad et al., 2000); shallow mesogenesis (depths 2–3 km, temperature 70–100 °C) and deep mesogenesis (depths >3 km, temperature >100 °C). Arumbera Sandstone diagenesis shows evidence for most aspects of the former, but limited aspects of the latter. Maximum burial depth based on diagenesis was, therefore, in the order of 3–4 km. Throughout burial, pore-water remained reducing and neutral-mildly alkaline, so the pyrite sole-veneer would have been retained through deep burial.

Authigenic kaolinite and illite commonly replace K-feldspar (Fig. 11, Eqs. (6) and (7)), during which both K^+ (and some Na^+ and Ca^{2+}) and SiO_2 are released into formation water, the former a source for illite formation, the latter for later quartz cementation. The dissolution of K-feldspar was the first mesodiagenetic event in the Arumbera Sandstone. If locally saturated with respect to K^+ then authigenic K-feldspar is an early re-precipitate in open pores (e.g., 'tooth-like' overgrowths Fig. 8c). The K-feldspar to illite reaction (Eq. (7)) occurs at the lower end of the temperature requirements for quartz cementation (70–80 °C). At higher temperatures (*c*.125 °C) K-feldspar often reacts with any available authigenic kaolinite to form illite and releases further SiO_2 for later quartz cementation (Eq. (8)). Kaolinite formation requires acidic pore-water and low K^+ activity, whereas illite formation needs neutral-mildly alkaline conditions and high K^+. The presence of illite and absence of kaolinite from the Arumbera Sandstone confirm pH was neutral-mildly alkaline.

The next major mesodiagenetic event for the Arumbera Sandstone was the transformation of both original detrital smectite and/or subsequent authigenic smectite into authigenic illite (Fig. 9d) and probably smectite-illite mixed layered clay; evidence is only observed for the former. These alterations proceed via dissolution-precipitation reactions, rather than by solid-state (Rask et al., 1997), and consume available K^+ from earlier K-feldspar dissolution, but release considerable cations Na^+, Ca^{2+}, Fe^{2+} and Mg^{2+} for subsequent mesodiagenetic changes (e.g., albitization, dolomite and chlorite) as well as SiO_2 for later quartz overgrowths. The reaction smectite to illite (Fig. 11, Eq. (9)) confirms that conditions remained neutral-mildly alkaline.

At slightly higher temperature and depth, smectite transforms to smectite-chlorite mixed layered clay (Fig. 11, Eq. (10)). Mg^{2+}-smectite is prone to chloritization and reflects a volcanic source (Chang et al., 1986). Again this is a dissolution–precipitation reaction. For the Arumbera Sandstone the occurrence of smectite–chlorite mixed-layer is confirmed by XRD analyses (Fig. 10). Mg^{2+} and Fe^{2+} from the earlier smectite to illite transformation is used in forming chlorite, K^+ utilisation is exhausted, whilst further Ca^{2+}, Na^+, SiO_2 and H_2O are released into the pore-water. Chlorite formation thus confirms pore-water pH remained neutral-mildly alkaline.

Albitization of plagioclase feldspar favours neutral pH, $Na^+ > Ca^{2+}$, uses previously released Na^+, can gen-

erate kaolinite, and releases excess Ca^{2+} as a by-product (Fig. 11, Eq. (11)). Any kaolinite generated transforms to illite at these deeper burial depths (Eq. (8)).

Authigenic overgrowth of quartz provided the main lithification event affecting the Arumbera Sandstone, developed either as euhedral overgrowths into open pores or more generally as anhedral overgrowths filling the remaining pore space after authigenic feldspar and clay transformations (Fig. 8c). It is relatively late in the mesodiagenetic sequence. Quartz can be precipitated over a wide range of temperatures (75–150 °C, Primmer et al., 1997), but generally indicates burial to at least 3 km and >100 °C. Silica is transferred by diffusion between sites of silica dissolution and precipitation at an interstitial scale. Intergranular pressure dissolution, or even stylolitization, is not extensive in the Arumbera Sandstone as a source for silica. The main silica sources are the series of preceding mesodiagenetic reactions (Fig. 11, Eqs. (6)–(10)), though an external source from adjacent mudrocks is also possible (cf. Gluyas et al., 2000).

Blocky, semi-poikilotopic, late dolomite cement occurs in Member III samples corroding detrital grains and earlier authigenic quartz overgrowths (Fig. 8e and f). Mesogenetic precipitation of carbonate cement in sandstone that post-dates quartz overgrowth relates to the different temperature-related solubility of the two minerals (Morad et al., 2000) and increased alkalinity yields carbonate cementation. With increase in temperature quartz shows progressive solubility, whereas carbonate minerals have a retrogressive solubility. Therefore, during progressive Arumbera Sandstone burial quartz becomes more soluble whereas carbonates tend to precipitate.

Other Australian examples exist of late mesogenetic carbonate cement (Schulz-Rojahn, 1993), where a cross-formational carbonate source is inferred. There is no shortage of local cross-formational dolomite sources for the Arumbera Sandstone; it is underlain and overlain by the Julie Formation dolomite and Todd River Dolomite, respectively. Moreover, the earlier mineral transformations (Fig. 11, Eqs. (9)–(11)) release Ca^{2+} and Mg^{2+} cations into the pore-water system which could all be taken up during mesogenetic dolomite formation.

Minor occurrences of chlorite platelets replacing detrital grains (Fig. 9g) indicate deepest burial of the Arumbera Sandstone. Furthermore, an increase in Mg^{2+} content in biotite at this 'chlorite' burial limit may be indicated by the green tinge of phlogopite.

The basic petrography presented here concurs with the regional reservoir findings of Lindsay and Gorter (1992), except they record 10% anhydrite in their samples. However, they quote earlier (1980) unpublished petrographic work by an oil company consultant, whose early diagenetic quartz overgrowths, early poikilotopic dolomite, late feldspar overgrowths and late authigenic clays cannot be reconciled with the sequential diagenetic history reported here.

5.8. Telodiagenesis

The Australian continent experienced subaerial weathering for hundreds of millions of years and can rightly claim to be the '*old continent*' (Twidale, 2000, p. 537). The only significant break in its subaerial history was a short-lived Aptian marine transgression across 45% of the continent (Twidale, 1994), which preserved in unconformity extensive tracts of the pre-existing Gondwana landscape (Twidale, 2000). Exhumed palaeolandscapes are recognised in the Cretaceous, Jurassic and Triassic; an earlier Carboniferous landscape is tentatively recognised (Bird and Chivas, 1993; Twidale, 1994, 2000; Tonui and De Caritat, 2003). By the late Jurassic, for example, much of the Australian part of Gondwana was reduced to an inselberg landscape (Twidale, 1994). Through these periods thick regolith developed that was subsequently lost through erosion.

The present Australian landscape is also of considerable antiquity, with thick regolith cover from prolonged and intense weathering (Taylor and Shirtliff, 2003), that extends for tens (perhaps hundreds) of meters below the surface, especially in porous rocks which stand in high relief. Whether or not the Arumbera Sandstone experienced the influence of near surface meteoric pore-water flushing during any particular palaeo-landscape development is not known, though higher ridges of the Macdonnell Ranges were exposed in Cretaceous landscapes (Twidale, 2000). For this discussion it is presumed the present day deep regolith is the main influence on Arumbera Sandstone telodiagenesis.

The transformation of the pyrite sole-veneer into the iron oxide-hydroxide seen at the present surface indicates a marked change in pore-water chemistry through meteoric pore-water flushing within the deep regolith. The anoxic and neutral-mildly alkaline pore-water carried through mesodiagenesis is gradually overtaken by an advancing front of oxic mildly acidic pore-water. Weathering intensity is greatest at the surface where weathering is oldest and most advanced, becoming less so with depth to the younger newly weathered zones.

Iron oxide transformations are complex with multifarious outcomes depending mainly on pH, Eh and temperature. Haematite is the ultimate end product. The reactions are two-fold, initial oxidation of pyrite followed by hydrolysis. The initial oxidation is well documented (Fig. 11, Eqs. (12) and (13)) where oxidation

reactions start and finish with ferrous-Fe^{2+}. According to Rimstidt and Vaughan (2003) the reaction does not oxidise iron, but rather it oxidises sulphur, where Fe^{2+} in solid-phase pyrite transforms to Fe^{2+} in solution, and sulphate SO_4^{2-} is the oxidation product. Hydrolysis then converts the ferrous-Fe^{2+} to ferric-Fe^{3+} in an aqueous ferrous-Fe^{2+} system (Eqs. (14) and (15)). These reactions are not as straightforward as it first appears, as the ferric-Fe^{3+} mineral formation is via a ferrihydrite precursor (referred to as amorphous hydrous ferric oxide) that is not yet fully understood, has a range of compositions in a ferrihydrite series, and is metastable so transforms spontaneously to haematite and goethite (Schwertmann et al., 1999). Hydrolysis continues once the ferric-Fe^{3+} system is established (Eqs. (16) and (17)), whereupon goethite dehydrates readily to haematite (Eq. (18)).

6. Discussion

6.1. Organic or pseudofossil origin

A non-biological pseudofossil sedimentary origin is assigned to some Neoproterozoic discoid features (Sun, 1986; Farmer et al., 1992). However, Gehling et al. (2000) repeatedly address the arguments for a pseudofossil interpretation in their detailed analysis of the discoid fossil *Aspidella* from southeastern Newfoundland. They weigh the evidence for inorganic against organic origin from a study of thousands of individual discoids to determine size and bedding surface distribution, variation in discoid shape and cross-section, and co-occurrence with recognised Ediacaran body fossils. They conclude that *Aspidella* and the array of synonymous forms within their *Aspidella*-plexus are body fossils where variation is due to body size and sedimentary condition.

The low diversity discoid specimens discovered and examined here from the Arumbera Sandstone display many of the characteristics that indicate an organic origin by Gehling et al. (2000). Conversely, it is tempting to dismiss them as gas-fluid escape sedimentary structures based simply on the occurrence of an internal sub-vertical disturbed zone with similarities to those displayed by Sun (1986) and Farmer et al. (1992). Arumbera Sandstone examples display collapsed internal ripple lamination with accompanying migration of the originally asymptotic basal contact to an acute angle contact. The collapse was clearly a single event (rather than chaotic collapse) with the ripple structure filling the vacancy left by the decayed holdfast bulb, which must have been filled during life with a low resistant fluid, perhaps just water. It also suggests the holdfast bulb was essentially the same scale as an individual ripple structure.

The most convincing argument against an inorganic gas-fluid escape origin for Arumbera Sandstone specimens is that it is extremely unlikely that a gas-fluid would build up and escape from the central (lowest) part of the discoid's V-shaped section. As with all sedimentary rocks pore fluid first migrates up-dip, in this case laterally up the V-shaped impermeable microbial lower surface, to escape from a 'higher' location, especially in a laminated microbial mat-rich sedimentary fabric where horizontal permeability greatly exceeds vertical permeability ($Kh > Kv$). Gas-fluid escape is also unlikely to maintain a parallel sided column (cf. Farmer et al., 1992), but would expand upwards in a bubble-like form (cf. Sun, 1986) where internal lamination heaves upward (cf. Farmer et al., 1992) rather than downward collapse (Fig. 6e). We also note that upward deflection of sedimentary laminae is common in escape burrows, in upward burrowing when forming a U-tube, and as an artefact during differential compaction of a sand-filled tube in a mud-rich medium.

The present authors firmly support a holdfast-bulb origin for Arumbera Sandstone discoids, wherein the sub-vertical disturbed zone represents the lower part of a decayed stalk following collapse of a decayed fluid filled bulb. Pseudofossil Kullingia scratch circles (Fig. 4j and k) indirectly attest the presence of frondose-like organisms or possibly seaweed swirling back and forth in tidal and wave currents on a firmground surface.

6.2. Aspidella plexus

The small type-*Aspidella* form (located at the apex of the *Aspidella* plexus) is not so far recognised in the relatively coarse-grained Arumbera Sandstone at Wyeecha Spring. The biomass analysis of *Aspidella* from Newfoundland by Gehling et al. (2000) indicates that the biota there is dominated by these small type-*Aspidella* morphs. It seems entirely possible that the *Aspidella* plexus is not in fact a simple equal tripartite grouping, but rather the type-*Aspidella* apex represents small juvenile forms growing on the sea-bed in a numerical majority that were regularly swept away by storm currents and hence not fossilised. Only a minority remained intact attached to the sticky microbial mat to grow to adulthood as the *Ediacaria* or *Spriggia* form-genera. It is also possible the proposed *Aspidella* plexus may hide a significant amount of true diversity given the morphological simplicity of early discoid forms (McIlroy et al., 2005), or there could be a true difference in taxonomic makeup of the Amadeus Basin material.

6.3. Palaeoenvironment and lithofacies associations

The lithology of the fossiliferous Member III of the Arumbera Sandstone, though not currently formally described in terms of lithofacies associations, is similar to Gehling's (2000) '*Facies Association F: interbedded siltstone and fossil bearing sandstone*' described from the high diversity Ediacara Member in neighbouring South Australia, as well as to Grazhdankin's (2004) '*interstratified sandstone and shale*' from the Vendian Group in the White Sea. Moreover, the similarities between the broad depositional setting of fossil bearing strata in the White Sea (Grazhdankin, 2004), the Flinders Ranges (Gehling, 2000) and the Arumbera Sandstone in the Amadeus Basin are striking.

Both the Gehling (2000) and Grazhdankin (2004) facies associations interpret deposition in a prodelta setting between storm and fair weather wave-base. Long periods of fair weather allowed colonization of the seabed by a benthic epifauna held in place by a mucilagenous microbial mat. Periodic storm surge sands inundated the benthic community, smothering and preserving whole colonies. Discoid holdfasts were not uprooted by these storm events, and remained attached to their biofilm. The same prodelta interpretation is proferred for the lowermost Member III of the Arumbera Sandstone (Fig. 2), in preference to the previous basinal designation (Lindsay, 1987; Lindsay and Gorter, 1992).

6.4. Diagenetic implications for palaeobiology

The diagenetic history of the Arumbera Sandstone indicates that haematite, and by analogy goethite, are late diagenetic developments. The case is argued that the original pyrite sole-veneer remained as pyrite for hundreds of millions of years through eo- and mesodiagenesis. Through deepest burial and gradual climb back towards the surface, pore-waters within the Arumbera Sandstone remained anoxic and neutral-mildly alkaline. Meteoric pore-water flushing within the deep regolith during late telodiagenesis (or perhaps also during periods of palaeo-landscape formation) introduced oxic and slightly acidic pore-water whereupon the pyrite sole-veneer was oxidised and hydrolysed to the haematite coating seen today in hand specimen and thin section.

The diagenetic history presented herein applies specifically to the Arumbera Sandstone deposited in the continually subsiding Ooraminna Sub-basin. Oxic conditions did not reach deposits subsiding in the sub-basin. Even sea-bed sediments a few cm deep (normally oxic) were anoxic due to the sealing effect of the surface microbial mat. Elsewhere within the Amadeus Basin, for example on the shallower and at times exposed Missionary Plain Trough, oxygenated seawater probably penetrated the Arumbera Sandstone during eodiagenesis, thus destroying any pyrite sole-veneer developed and its potential for fossilisation; a different diagenetic history applies. The absence of Members III and IV over the Missionary Plain Trough is testimony to sub-aerial exposure. Consequently, the applicability of the Gehling (1999) preservation model is higher in areas where subsidence after anoxic deposition was continuous and relatively rapid.

7. Conclusion

An Ediacaran discoid fauna is reported from the Neoproterozoic–Cambrian Arumbera Sandstone (Members II and III) in the Amadeus Basin. The biota is associated with periodic storm-event beds, and the presence of wrinkle structures from a range of localities and facies attest to the former presence of microbial mats.

Thin sections through discoids reveal both subparallel bedding laminae and ripple foresets within the fossil body. A thin (<1 mm) hyporelief coating of clay, haematite and fine silt appears superficial to the fine-grained sand body fill, and probably represents the remains of the microbial mat. Furthermore, a sub-vertical disturbed zone through the discoid fossil body is interpreted as the location of the lower part of a decayed stalk following collapse of a decayed holdfast-bulb. A step-by-step sequence of sedimentation events concurs with, and advances, a slightly modified Gehling (1999) model. No direct evidence of a pyrite sole-veneer is observed for the Arumbera Sandstone.

Detailed petrography unravels a diagenetic history that demonstrates the importance of a pyrite sole-veneer by tracing its passage through a sequence of diagenetic events to the haematite coating seen today. Anoxic and alkaline conditions continued during subsidence after syn-depositional formation of the pyrite sole-veneer; thus its retention through eodiagenesis. Mesodiagenetic events, particularly clay mineral transformations, confirm pore-water remained anoxic and neutral-mildly alkaline, so the pyrite sole-veneer remained intact through deepest burial. The advance of meteoric water through the present deep regolith marks a late telodiagenetic change to oxic and mildly acidic pore-water. The pyrite sole-veneer was firstly oxidised and then hydrolysed to haematite. A diagenetic linkage between the present haematite coating and a syn-depositional pyrite sole-veneer is established, and thus the Gehling (1999) preservation model is feasible and likely during a

Neoproterozoic taphonomic window prior to metazoan bioturbation and cropping in the Cambrian.

The interpreted diagenetic history is specific to the distal marine shelf sediments of the Arumbera Sandstone in the Ooraminna Sub-basin (and by analogy to other subsiding basins in the Neoproterozoic). The applicability of Gehling's (1999) model and Narbonne's (2005) Flinders-style preservation are higher where subsidence was continuous and relatively rapid. In shallower or eroded parts of the Amadeus Basin (e.g., Missionary Plain Trough) that may have experienced intermittent or patchy infiltration by eogenetic oxic water, diagenetic history was different and Ediacaran fossils less likely preserved. Ediacaran preservation, therefore, is as much a function of diagenetic history as it is of depositional environment.

Acknowledgements

We thank Mr. Ken Paige (owner, Todd River cattle station, NT) for access and permission to sample, Dr. Robert Jones (Australian Museum Sydney) for export permit for BM, Drs. Charlie Underwood, Andy Beard and Steve Hirons (Birkbeck University of London) for discussion, SEM and XRD analyses, and Gillian Mapstone and Caroline McIlroy for field assistance. Both authors acknowledge financial support from the Percy Sladen Memorial Fund (The Linnean Society of London) towards fieldwork costs. Initial fieldwork conducted by DM was during tenure of a Royal Society Fellowship at Macquarrie University, Sydney, and the interpretation completed with assistance from Canada Research Chairs Program.

References

Allen, R.E., 2002. Role of diffusion-precipitation reactions in authigenic pyritization. Chem. Geol. 182, 461–472.

Bartley, J.K., Pope, M., Knoll, A.H., Semikhatov, M.A., Petrov, P.Y., 1998. A Vendian–Cambrian boundary succession from the northwestern margin of the Siberian Platform: stratigraphy, palaeontology, chemostratigraphy and correlation. Geol. Mag. 135, 473–494.

Berner, R.A., 1981. A new geochemical classification of sedimentary environments. J. Sediment. Petrol. 51, 359–365.

Berner, R.A., 1994. 3GEOCARB II: a revised model of atmospheric CO_2 over Phanerozoic time. Am. J. Sci. 294, 56–91.

Billings, E., 1872. Fossils in Huronian rocks. Can. Nat. Quart. J. Sci. 6, 478.

Bird, M.I., Chivas, A.R., 1993. Geomorphic and palaeoclimatic implications of an oxygen-isotope chronology for Australian deeply weathered profiles. Aust. J. Earth Sci. 40, 345–358.

Bouougri, E., Porada, H., 2002. Mat-related sedimentary structures in Neoproterozoic peritidal passive margin deposits of the West African Craton (Anti-Atlas, Morocco). Sediment. Geol. 153, 85–106.

Brasier, M.D., 1992. Global ocean-atmosphere change across the Precambrian–Cambrian transition. Geol. Mag. 129, 161–168.

Brasier, M., Antcliffe, J., 2004. Decoding the Ediacaran enigma. Science 305, 1115–1117.

Briggs, D.E.G., Raiswell, R., Bottrell, S.H., Hatfield, D., Bartels, C., 1996. Controls on the pyritization of exceptionally preserved fossils: an analysis of the Lower Devonian Hunsrück Slate of Germany. Am. J. Sci. 296, 633–663.

Buss, L.W., Seilacher, A., 1994. The Phylum Vendobionta: a sister group of the Eumetazoa? Paleobiology 20, 1–4.

Butler, I.B., Rickard, D., 2000. Framboidal pyrite formation via the oxidation of iron (II) monosulfide by hydrogen sulphide. Geochim. Cosmochim. Acta 64, 2665–2672.

Canfield, D.E., Raiswell, R., 1991. Pyrite formation and fossil preservation. In: Allison, P.A., Briggs, D.E.G. (Eds.), Taphonomy: Releasing the Data Locked in the Fossil Record. Plenus Press, New York, pp. 337–387.

Canfield, D.E., Thamdrup, B., Fleischer, S., 1998. Isotope fractionation and sulphur metabolism by pure and enrichment cultures of elemental sulphur-disproportionating bacteria. Limnol. Oceanogr. 43, 253–264.

Chang, H.K., Mackenzie, F.T., Schoonmaker, J., 1986. Comparisons between the diagenesis of dioctahedral and trioctahedral smectite, Brazilian offshore basins. Clays Clay Mineral. 34, 407–423.

Cornell, R.M., Schwertmann, U., 1996. The Iron Oxides: Structure, Properties, Reactions, Occurrence and Uses. Weinheim, New York, 573 pp.

Dalziel, I.W.D., 1997. Neoproterozoic–Paleozoic geography and tectonics: review, hypothesis, environmental speculation. Geol. Soc. Am. Bull. 109, 16–42.

Dzik, J., 2003. Anatomical information content in the Ediacaran fossils and their possible zoological affinities. Interact. Comp. Biol. 43, 114–126.

Farmer, J., Vidal, G., Moczydlowska, M., Strauss, H., Ahlberg, P., Siedlecka, A., 1992. Ediacaran fossils from the Innerelv Member (late Proterozoic) of the Tanafjorden area, northeastern Finnmark. Geol. Mag. 129, 181–195.

Føyn, S., Glaessner, M.F., 1979. *Platysolenites*, other animal fossils, and the Precambrian–Cambrian transition in Norway. Norsk Geologisk Tidssk 59, 25–46.

Gehling, J.G., 1987. Earliest known echinoderm—a new Ediacaran fossil from the Pound Subgroup of South Australia. Alcheringa 11, 337–345.

Gehling, J.G., 1991. The case for Ediacaran fossil roots to the metazoan tree. Geol. Soc. India Mem. 20, 181–224.

Gehling, J.G., 1999. Microbial mats in terminal Proterozoic siliciclastics: Ediacaran death masks. Palaios 14, 40–57.

Gehling, J.G., 2000. Environmental interpretation and a sequence stratigraphic framework for the terminal Proterozoic Ediacara Member within the Rawnsley Quartzite, South Australia. Precamb. Res. 100, 65–95.

Gehling, J.G., Narbonne, G.M., Anderson, M.M., 2000. The first named Ediacaran body fossil, *Aspidella terranovica*. Palaeontology 43, 427–456.

Glaessner, M.F., 1959. Precambrian Coelenterata from Australia, Africa and England. Nature 183, 1472–1473.

Glaessner, M.F., 1969. Trace fossils from the Precambrian and basal Cambrian. Lethaia 2, 369–393.

Glaessner, M.F., 1979. Precambrian. In: Robinson, R.A., Teichert, C. (Eds.), Treatise on Invertebrate Paleontology. Part A. Introduction, Fossilization (Taphonomy), Biogeography and Biostratigraphy.

Geological Society of America & University of Kansas, Lawrence, pp. A79–A118.
Glaessner, M.F., 1984. The Dawn of Animal Life. A Biohistorical Study. Cambridge University Press, 244 pp.
Glaessner, M.F., Wade, M., 1966. The late Precambrian fossils from Ediacara, South Australia. Palaeontology 9, 599–628.
Glaessner, M.F., Walter, M.R., 1975. New Precambrian fossils from the Arumbera Sandstone, Northern Territory, Australia. Alcheringa 1, 11–28.
Gluyas, J.G., Garland, C., Oxtoby, N.H., Hogg, A.J.C., 2000. Quartz cement; the Millar's Tale. In: Worden, R.H., Morad, S., (Eds.), Quartz Cementation in Sandstones. International Association of Sedimentologists, Special Publication 29, pp. 199–217.
Grazhdankin, D., 2004. Patterns of distribution in the Ediacaran biotas: facies versus biogeography and evolution. Paleobiology 30, 203–221.
Grimes, S.T., Brock, F., Rickard, D., Davies, K.L., Edwards, D., Briggs, D.E.G., Parkes, R.J., 2001. Understanding fossilization: experimental pyritization of plants. Geology 29, 123–126.
Grimes, S.T., Davies, K.L., Butler, I.B., Brock, F., Edwards, D., Rickard, D., Briggs, D.E.G., Parkes, R.J., 2002. Fossil plants from the Eocene London Clay: the use of pyrite textures to determine the mechanism of pyritization. J. Geol. Soc. Lond. 159, 493–501.
Hagadorn, J.W., Bottjer, D.J., 1997. Wrinkle structures: microbially mediated sedimentary structures in siliciclastic settings at the Proterozoic–Phanerozoic transition. Geology 25, 1047–1050.
Hagadorn, J.W., Bottjer, D.J., 1999. Restriction of a late Neoproterozoic biotope: suspect-microbial structures and trace fossils at the Vendian–Cambrian transition. Palaios 14, 73–85.
Herbert Jr, R.B., Benner, S.G., Pratt, A.R., Blowes, D.W., 1998. Surface chemistry and morphology of poorly crystalline iron sulfides precipitated in media containing sulphate-reducing bacteria. Chem. Geol. 144, 87–97.
Hoffman, P.F., Kaufman, A.J., Halverson, G.P., Schrag, D.P., 1998. A Neoproterozoic snowball Earth. Science 281, 1342–1346.
Hyde, W.T., Crowley, T.J., Baum, S.K., Peltier, W.R., 2000. Neoproterozoic 'snowball Earth' simulations with a coupled climate/ice-sheet model. Nature 405, 425–429.
Jenkins, R.J.F., 1992. Functional and ecological aspects of Ediacaran assemblages. In: Lipps, J.H., Signor, P.W. (Eds.), Origin and Early Evolution of the Metazoa. Plenum Press, New York, pp. 131–176.
Jenkins, R.J.F., 1995. The problems and potential of using animal fossils and trace fossils in terminal Proterozoic stratigraphy. Precamb. Res. 73, 51–69.
Jenkins, R.J.F., Gehling, J.G., 1978. A review of the frond-like fossils of the Ediacara assemblage. Rec. South Aust. Museum 17, 347–359.
Jensen, S., Gehling, J.G., Droser, M.L., 1998. Ediacara-type fossils in Cambrian sediments. Nature 393, 567–569.
Jensen, S., Gehling, J.G., Droser, M.L., Grant, S.W.F., 2002. A scratch circle origin for the medusoid fossil *Kullingia*. Lethaia 35, 291–299.
Kennard, J.M., Nicoll, R.S., Owen, M., 1986. Late Proterozoic and early Palaeozoic depositional facies of the Northern Amadeus Basin, central Australia. In: Proceedings of the 12th International Sedimentological Congress Field Excursion 25B, Bureau of Mineral Resources, Geology and Geophysics, Canberra, 124 pp.
Knoll, A.H., Walter, M.R., 1992. Latest Proterozoic stratigraphy and Earth history. Nature 356, 673–678.
Knoll, A.H., Walter, M.R., Narbonne, G.M., Christie-Blick, N., 2004. A new period for the geologic time scale. Science 305, 621–622.
LaFlamme, M., Narbonne, G.M., Anderson, M.M., 2004. Morphometric analysis of the Ediacaran frond *Charniodiscus* from the Mistaken Point Formation, Newfoundland. J. Paleontol. 78, 827–837.
Lindsay, J.F., 1987. Sequence stratigraphy and depositional controls in late Proterozoic-early Cambrian sediments of the Amadeus Basin, central Australia. Am. Assoc. Petroleum Geol. Bull. 71, 1387–1403.
Lindsay, J.F. (Ed.), 1993. Geological Atlas of the Amadeus Basin. Australian Geological Survey Organisation, Canberra, 25 plates.
Lindsay, J.F., Korsch, R.J., 1989. Interplay of tectonics and sea-level changes in basin evolution: an example from the intracratonic Amadeus Basin, central Australia. Basin Res. 2, 3–25.
Lindsay, J.F., Korsch, R.J., 1991. The evolution of the Amadeus Basin, central Australia. In: Korsch, R.J., Kennard, J.M., (Eds.), Geological and Geophysical Studies in the Amadeus Basin, central Australia. Bureau of Mineral Resources Geology and Geophysics, Australia, Bulletin, 236, pp. 7–32.
Lindsay, J.F., Gorter, J.D., 1992. Clastic petroleum reservoirs of the late Proterozoic and early Paleozoic Amadeus Basin, central Australia. In: Rhodes, E.G., Moslow, T. (Eds.), Marine Clastic Reservoirs: Examples and Analogs. Springer-Verlag, New York, pp. 39–74.
Lindsay, J.F., Korsch, R.J., Wilford, J.R., 1987. Timing the breakup of a Proterozoic supercontinent: evidence from Australian intracratonic basins. Geology 15, 1061–1064.
Loope, D.B., Watkins, D.K., 1989. Pennsylvanian fossils replaced by red chert: early oxidation of pyrite precursors. J. Sediment. Petrol. 59, 375–386.
McIlroy, D., Walter, M.R., 1997. A reconsideration of the biogenicity of *Arumberia banksi* Glaessner and Walter. Alcheringa 21, 79–80.
McIlroy, D., Jenkins, R.J.F., Walter, M.R., 1997. The nature of the Proterozoic–Cambrian transition in the northern Amadeus Basin, central Australia. Precamb. Res. 86, 93–113.
McIlroy, D., Crimes, T.P., Pauley, J.C., 2005. Fossils and matgrounds from the Neoproterozoic Longmyndian Supergroup, Shropshire, UK. Geol. Mag. 142, 441–455.
Meert, J.G., Lieberman, B.S., 2004. A palaeomagnetic and palaeobiogeographical perspective on latest Neoproterozoic and early Cambrian tectonic events. J. Geol. Soc. Lond. 161, 477–487.
Morad, S., Ketzer, J.M., De Ros, L.F., 2000. Spacial and temporal distribution of diagenetic alterations in siliciclastic rocks: implications for mass transfer in sedimentary basins. Sedimentology 47, 95–120.
Narbonne, G.M., 1998. The Ediacara biota: a terminal Neoproterozoic experiment in the evolution of life. GSA Today 8, 1–6.
Narbonne, G.M., 2004. Modular construction of early Ediacaran complex life forms. Science 305, 1141–1144.
Narbonne, G.M., 2005. The Ediacara biota: Neoproterozoic origin of animals and their ecosystems. Annu. Rev. Earth Planet. Sci. 33, 421–442.
Needham, S.J., Worden, R.H., McIlroy, D., 2005. Experimental production of clay rims by macrobiotic sediment ingestion and excretion processes. J. Sediment. Res. 75, 1028–1037.
Noffke, N., Knoll, A.H., Grotzinger, J.P., 2002. Sedimentary controls on the formation and preservation of microbial mats in siliciclastic deposits: a case study from the upper Neoproterozoic Nama Group, Namibia. Palaios 17, 533–544.
Oaks, R.Q. Jn., Deckelman, J.A., Conrad, K.T., Hamp, L.T., Phillips, J.O., Stewart, A.J., 1991. Sedimentation and tectonics in the northwestern and central Amadeus Basin, central Australia In: Korsch, R.J., Kennard, J.M., (Eds.), Geological and Geophysical Studies in the Amadeus Basin, central Australia. Bureau of Mineral Resources Geology and Geophysics Australia, Bulletin 236, pp. 73–90.

Ottonello, G., 1997. Principles of Geochemistry. Columbia University Press, New York, 894 pp.

Pettijohn, F.J., Potter, P.E., Siever, R., 1987. Sand and Sandstone, 2nd ed. Springer-Verlag, New York, 553 pp.

Primmer, T.J., Cade, C.A., Evans, J., Gluyas, J.G., Hopkins, M.S., Oxtoby, N.H., Smalley, P.C., Warren, E.A., Worden, R.H., 1997. Global patterns in sandstone diagenesis: their application to reservoir quality prediction for petroleum exploration. In: Kupecz, J.A., Gluyas, J., Bloch, S. (Eds.), Reservoir Quality Prediction in Sandstones and Carbonates. American Association of Petroleum Geologists Memoir 69, pp. 61–77.

Rask, J.H., Bryndzia, L.T., Braunsdorf, N.R., Murray, T.E., 1997. Smectite illitization in Pliocene-age Gulf of Mexico mudrocks. Clays Clay Mineral. 45, 99–109.

Rickard, D.T., 1995. Kinetics of FeS precipitation: Part I. Competing reaction mechanisms. Geochim. Cosmochim. Acta 59, 4367–4379.

Rimstidt, J.D., Vaughan, D.J., 2003. Pyrite oxidation: a state-of-the-art assessment of the reaction mechanism. Geochim. Cosmochim. Acta 67, 873–880.

Schaefer, B.F., Burgess, J.M., 2003. Re-Os isotope age constraints on deposition in the Neoproterozoic Amadeus Basin: implications for the 'Snowball Earth'. J. Geol. Soc. Lond. 160, 825–828.

Schieber, J., 1998. Possible indicators of microbial mat deposits in shales and sandstones: examples from the mid-Proterozoic Belt Supergoup, Montana, USA. Sediment. Geol. 120, 105–124.

Schieber, J., 1999. Microbial mats in terrigenous clastics: the challenge of identification in the rock record. Palaios 14, 3–12.

Schoonen, M.A.A., 2004. Mechanisms of sedimentary pyrite formation. In: Amend, J.P., Edwards, K.J., Lyons, T.W. (Eds.), Sulfur Biogeochemistry—Past and Present, 379. Geological Society of America, pp. 117–134, Special Paper.

Schoonen, M.A.A., Barnes, H.L., 1991. Reactions forming pyrite and marcasite from solution: II. Via FeS precursors below 100 °C. Geochim. Cosmochim. Acta 55, 1505–1514.

Schulz-Rojahn, J.P., 1993. Calcite-cemented zones in the Eromanga Basin: clues to petroleum migration and entrapment? Aust. Petroleum Explor. Assoc. J. 33, 63–76.

Schwertmann, U., Friedl, J., Stanjek, H., 1999. From Fe(III) ions to ferrihydrite and then to hematite. J. Colloid Interface Sci. 209, 215–223.

Seilacher, A., 1984. Late Precambrian and Early Cambrian Metazoa: preservational or real extinctions? In: Holland, R.D., Trendall, A.F. (Eds.), Patterns of Change in Earth Evolution. Springer-Verlag, Berlin, pp. 159–168.

Seilacher, A., 1989. Vendozoa: organismic construction in the Proterozoic biosphere. Lethaia 22, 229–239.

Seilacher, A., 1992. Vendobionta and Psammocorallia: lost constructions of Precambrian evolution. J. Geol. Soc. Lond. 149, 607–613.

Seilacher, A., 1999. Biomat-related lifestyles in the Precambrian. Palaios 14, 86–93.

Shaw, R.D., 1991. The tectonic development of the Amadeus Basin, central Australia. In: Korsch, R.J., Kennard, J.M., (Eds.), Geological and Geophysical Studies in the Amadeus Basin, central Australia. Bureau of Mineral Resources Geology and Geophysics Australia, Bulletin 236, pp. 429–461.

Shergold, J.H., 1991. Late Proterozoic and early Palaeozoic palaeontology and biostratigraphy of the Amadeus Basin. In: Korsch, R.J., Kennard, J.M., (Eds.), Geological and Geophysical Studies in the Amadeus Basin, central Australia. Bureau of Mineral Resources Geology and Geophysics Australia, Bulletin 236, pp. 97–111.

Shu, D.-G., Conway Morris, S., Han, J., Li, Y., Zhang, X.-L., Hua, H., Zhang, Z.-F., Liu, J.-N., Guo, J.-F., Yao, Y., Yasui, K., 2006. Lower Cambrian vendobionts from China and early diploblast evolution. Science 312, 731–734.

Sprigg, R.C., 1947. Early Cambrian (?) jellyfishes from the Flinders Ranges, South Australia. Trans. Roy. Soc. South Aust. 71, 212–224.

Sprigg, R.C., 1949. Early Cambrian "jellyfishes" of Ediacara, South Australia and Mount John, Kimberley District, Western Australia. Trans. Roy. Soc. South Aust. 73, 72–99.

Sun, W., 1986. Precambrian medusoids: the *Cyclomedusa* plexus and *Cyclomedusa*-like pseudofossils. Precamb. Res. 31, 325–360.

Sweeney, R.E., Kaplin, I.R., 1973. Pyrite framboid formation: laboratory synthesis and marine sediments. Econ. Geol. 68, 618–634.

Taylor, G., Shirtliff, G., 2003. Weathering: cyclical or continuous? An Australian perspective. Aust. J. Earth Sci. 50, 9–17.

Tonui, E., De Caritat, P., 2003. Composition, diagenesis, and weathering of the sediments and basement of the Callabonna Sub-basin, central Australia: implications for landscape evolution. J. Sediment. Res. 73, 1036–1050.

Tucker, M.E., 2001. Sedimentary Petrology: an Introduction to the Origin of Sedimentary Rocks, 3rd ed. Blackwell Science Ltd., Oxford, 262 pp.

Twidale, C.R., 1994. Gondwanan (Late Jurassic and Cretaceous) palaeosurfaces of the Australian craton. Palaeogeogr. Palaeoclimatol. Palaeoecol. 112, 157–186.

Twidale, C.R., 2000. Early Mesozoic (?Triassic) landscapes in Australia: evidence, argument, and implications. J. Geol. 108, 537–552.

Veevers, J.J., 2000. Neoproterozoic-Palaeozoic Australia & neighbours in Gondwanaland. In: Veevers, J.J. (Ed.), Billion-year Earth History of Australia and Neighbours in Gondwanaland. Gemoc Press, Sydney, pp. 253–281.

Wade, M., 1968. Preservation of soft-bodied animals in Precambrian sandstones at Ediacara, South Australia. Lethaia 1, 238–267.

Wade, M., 1969. Medusae from uppermost Precambrian or Cambrian sandstones, central Australia. Palaeontology 12, 351–365.

Wade, M., 1970. The stratigraphic distribution of the Ediacara fauna in Australia. Trans. Roy. Soc. South Aust. 94, 87–104.

Wade, M., 1972. Hydrozoa and Scyphozoa and other medusoids from the Precambrian Ediacara fauna, South Australia. Palaeontology 15, 197–225.

Waggoner, B., 2003. The Ediacaran biotas in space and time. Integr. Comp. Biol. 43, 104–113.

Walter, M.R., Veevers, J.J., 2000. Neoproterozoic Australia. In: Veevers, J.J. (Ed.), Billion-year Earth History of Australia and Neighbours in Gondwanaland. Gemoc Press, Sydney, pp. 131–153.

Wells, A.T., Ranford, L.C., Stewart, A.J., Cook, P.J., Shaw, R.D., 1967. Geology of the north-eastern part of the Amadeus Basin, Northern Territory. Bureau of Mineral Resources Geology and Geophysics, Australia, Report, 113, 97 pp.

Wells, A.T., Forman, D.J., Ranford, L.C., Cook, P.J., 1970. Geology of the Amadeus Basin, central Australia. Bureau of Mineral Resources Geology and Geophysics, Australia, Bulletin, 100, 222 pp.

Wilkin, R.T., Barnes, H.L., 1997. Formation processes of framboidal pyrite. Geochim. Cosmochim. Acta 61, 323–339.

Worden, R.H., Morad, S., 2000. Quartz cementation in oil field sandstones: a review of the key controversies. In: Worden, R.H., Morad, S. (Eds.) Quartz Cementation in Sandstones. International Association of Sedimentologists, Special Publication 29, pp. 1–20.

Xiao, S., Shen, B., Zhou, C., Xie, G., Yuan, X., 2005. A uniquely preserved Ediacaran fossil with direct evidence for a quilted bodyplan. Proc. Natl. Acad. Sci. U.S.A. 102, 10227–10232.